Timing of fluvial terrace formation and concomitant travertine deposition in the upper Sutlej River (Tirthapuri, southwestern Tibet) and paleoclimatic implications

Zhijun Wang [a], Michael C. Meyer [a, *], Luke A. Gliganic [a], Dirk L. Hoffmann [b], Jan-Hendrik May [c]

[a] Institute of Geology, University of Innsbruck, Innrain 52, A-6020 Innsbruck, Austria
[b] Department of Human Evolution, Max Planck Institute for Evolutionary Anthropology, D-04103 Leipzig, Germany
[c] Institute of Earth and Environmental Sciences - Geology, Albert-Ludwigs-Universität Freiburg, D-79098 Freiburg, Germany

ARTICLE INFO

ABSTRACT

Travertines are carbonates precipitated from hydrothermal springs and are relatively common on the Tibetan plateau and occur along tectonically active faults. The Karakoram fault system is an active strike-slip fault that extends from the Pamir into southwestern Tibet, where it controls the course of the upper Sutlej River and the occurrence of several hydrothermal springs, including the Tirthapuri hot springs. Multiple fluvial terraces that are partly capped by travertine are preserved in the Tirthapuri area. Four main fluvial terrace levels (labelled as T1 to T4 with increasing height above river) were identified and several meter-thick travertine platforms occur on the current river level as well as the T2 and T3 terraces. Sedimentological and petrographic observations suggest that the travertine platforms were deposited on active floodplains of the paleo- and modern Sutlej River, and preserved from fluvial erosion because travertine precipitation was immediately followed by vertical river-bed incision and thus terrace abandonment. Results of ^{230}Th/U in combination with luminescence dating show that the deposition of travertine platform and river incision that led to the formation of T3 terrace (~93 m above the Sutlej) took place at ca. 127.5 ka. The development of terrace T2 and overlying travertine platform (~28 m above the Sutlej) occurred between ca. 10.0 and 8.8 ka. Fluvial incision has arrived at the modern level at least ca. 0.2 ka ago. Both the travertine deposition and major river incision are likely triggered by the intensified Indian summer monsoon and are linked to phases of maximum monsoon strength. During strong monsoon phases, a large quantity of moisture is transported into southwestern Tibet, activating hot springs and thus travertine precipitation, facilitating fluvial incision and stripping off sediments from the regional hill-slopes. At least over the last glacial cycle we suggest that the Tirthapuri travertine and associated fluvial incision are sensitive indicators of (peak) monsoonal activity and can thus provide valuable insights into past climate change and climate-driven landscape evolution on the southwestern Tibetan Plateau. Comparison of our findings with published data further suggests that monsoon-controlled fluvial aggradation and incision during the early Holocene is synchronous in southwestern Tibet and the adjacent sector of the Himalayan orogen (north-western Sub-to High Himalaya).

© 2017 Elsevier Ltd. All rights reserved.

1. Introduction

Over the last decades fluvial terraces have been increasingly recognized as an important source of evidence for Quaternary climate change and tectonic movements (Maddy et al., 2001; Wegmann and Pazzaglia, 2002, 2009; Starkel, 2003; Bridgland and Westaway, 2008; Garcia and Mahan, 2014; Wang et al., 2015). Climate regulates fluvial discharge, vegetation cover and related variations in sediment supply and thus plays a fundamental role in alluvium aggradation and incision, ultimately controlling the formation of fluvial terraces over orbital (i.e. glacial-interglacial) and sub-orbital time-scales (Vandenberghe, 2002; Maddy et al., 2001; Bridgland and Westaway, 2008; Wang et al.,

* Corresponding author.
E-mail address: michael.meyer@uibk.ac.at (M.C. Meyer).

2015). Furthermore, many studies suggest that fluvial terraces have a combined tectonic-climatic origin, particularly in tectonically active regions (Maddy et al., 2001; Starkel, 2003; Wegmann and Pazzaglia, 2009; Wang et al., 2015; Dey et al., 2016).

In the Tibetan-Himalayan orogen, fluvial systems are operating against the background of (i) active tectonics that often entail pronounced rock- and surface uplift (Kirby et al., 2003; Vance et al., 2003; Finnegan et al., 2008) and (ii) spatio-temporal variations in the intensity of the Indian summer monsoon (ISM; e.g. Bookhagen et al., 2005; Murari et al., 2014; Cai et al., 2015; Kathayat et al., 2016). The vastness of the Tibetan-Himalayan orogen and the complexity of climate and tectonic interactions with the Earth's surface complicate a simple model for terrace formation and evolution to be put forward for High Asia yet. Furthermore, before disentangling any tectonic from climatic signals in a fluvial terrace succession, a basic geomorphic assessment of terrace type (e.g. erosional versus aggradational, paired versus unpaired) in combination with a reliable chronological framework is required for a genetic interpretation of terrace formation (Bridgland and Westaway, 2008; Schaller et al., 2016). Only a limited number of studies with good chronological control on successive fluvial terrace levels are currently available for the Tibetan-Himalayan orogen. This research suggests that on orbital time-scales rock uplift rates varied significantly and influenced terrace formation and preservation (Pan et al., 2009; Perrineau et al., 2011). On sub-orbital time-scales studies from the northeastern, southeastern as well as northern margins of Tibetan Plateau suggest that terrace aggradation occurred during cold periods characterized by a weak ISM, while fluvial down-cutting took place during transitions from weak to strong phases of ISM (Wang et al., 2009, 2015). This contrasts with terrace development in catchments that are under the direct influence of the ISM (i.e. the south-facing slopes of the Himalaya), where strong ISM enhances the sediment flux causing valley floor aggradation, while phases of weak ISM result in valley fill incision and terrace development (Bookhagen et al., 2006; Juyal et al., 2010; Dey et al., 2016).

In Tibet, pull-apart basins bound to major strike-slip faults (such as the Karakorum fault; Fig. 1B; Armijo et al., 1989; Zhang et al., 2010) or ~ N-S-trending rift systems (such as the Yadong-Gulu rift; Fig. 1B; Blisniuk et al., 2001; Taylor et al., 2003; Zhang et al., 2010; Ratschbacher et al., 2011) are common. In these basins, thick sequences composed of fluvial, lacustrine and alluvial fan sediments accumulated during Late Neogene to early Quaternary (Wang et al., 2008a,b; Kempf et al., 2009; Saylor et al., 2009; Zhang et al., 2010). Today these basins are often incised by the modern drainage network and characterized by a landscape that preserves multiple fluvial terraces (e.g. Wang et al., 2008a). For large areas of the Tibetan plateau — southern Tibet included — the timing and nature of fluvial incision into these tectonic basins and the associated formation of fluvial terraces are not well constrained (Brown et al., 2003; Finnegan et al., 2008; Kaiser et al., 2010; Zhu et al., 2014).

Travertine (i.e. a spring carbonate precipitated by hydrothermal water generally >30 °C, also referred to as hydrothermal carbonate; Capezzuoli et al., 2014) is a relatively common deposit on the Tibetan plateau and often occurs along faults that are associated with pull-apart and rift basins (Tong et al., 2000; Zentmyer et al., 2008; Wang et al., 2016). Such fault-bounded spring carbonates can be radiometrically dated via uranium-series disequilibrium dating techniques (e.g. ^{230}Th/U dating; Mallick and Frank, 2002; Sierralta et al., 2010; Wang et al., 2016; Meyer et al., 2017). In valley settings these spring carbonates are often stratigraphically associated with eolian, fluvial and other types of clastic deposits that are amenable to absolute dating techniques such as optically stimulated luminescence (OSL) dating, in combination allowing a

chronostratigraphic framework for travertine and clastic sediment activity to be established (Rich et al., 2003; Ruszkiczay-Rudiger et al., 2005; Mahan et al., 2007; Luque and Julia, 2007; Schulte et al., 2008; Zentmyer et al., 2008).

In this study the Tirthapuri travertine that is located in the upper Sutlej River in southwestern Tibet and that is stratigraphically linked with a staircase of fluvial terraces are investigated. The travertine deposit and the fluvial terraces formed in the Menci basin (a pull-apart basin that is bound to the Karakoram strike-slip fault) and hydrothermal spring carbonate can be found on multiple terrace levels. We combine geomorphological, sedimentological and petrological investigations as well as uranium-series (i.e. ^{230}Th/U) and OSL dating in order to (i) understand the depositional history of the travertine complex, (ii) elucidate the Late Quaternary evolution of the Menci basin that appears to have been dominated by fluvial incision, and (iii) decipher the relative importance of tectonic versus climatic forcing on fluvial incision and travertine formation.

2. Site description and geological setting

The Tirthapuri travertine is located 5 km south of the village of Menci in the homonymous Menci basin in the upper reaches of the Sutlej River (Fig. 1). Today a cold and dry continental climate with a mean annual air temperature of 0–3 °C and mean annual precipitation (MAP) of ~250 mm prevails in the investigation area (Li, 2006). The atmospheric circulation pattern in this region is affected by both the ISM and the winter westerlies (Bookhagen and Burbank, 2010; Yao et al., 2013). Time series analysis of radar data from 1998 to 2015 from the Tropical Rainfall Measuring Mission for the Menci basin (conducted by us) and for the southwestern Tibet (conducted by Bookhagen and Burbank, 2010) suggest that the ISM delivers ~70% of annual precipitation to the south western part of the Tibetan plateau (during June to September), whereas the westerlies contribute the remaining ~30% during the rest of the year.

At Tirthapuri, several active hot springs with a discharge rate of ~0.1–20 L/s emerge from the quartzite host rock or the modern floodplain of the Sutlej River (Tong et al., 2000). The main hot spring water has a temperature of ~72 °C and pH value of ~7 (Tong et al., 2000). Major ions in the spring water are HCO_3^- (689 mg/L), Na^+ (123 mg/L), SO_4^{2-} (89 mg/L), Ca^{2+} (74 mg/L) and Mg^{2+} (50 mg/L), whereas K^+ and Cl^- are of low concentrations (20–40 mg/L; Tong et al., 2000). The enrichment of Ca^{2+} and HCO_3^- ions in the spring water suggests that the hydrothermal water passed through a carbonate aquifer (probably the Mesozoic limestone underlying the Menci basin; Fig. 1C; Tong et al., 2000; Wang et al., 2008a). Bedrock outcrops adjacent to the Tirthapuri hot spring are composed of quartzite that probably belongs to the Tethyan metasedimentary sequence and has locally been altered by the hydrothermal activity.

The Menci basin is ~40 km long ~15 km wide and one of several basins (like the Barga and the Zhada to the east and west, respectively) that trends in NW-SE direction and roughly parallels the Indus-Yarlung Tsangpo suture (IYS) zone (Fig. 1C). The IYS resulted from the main India-Eurasia collision at ca. 50 Ma ago (Hodges, 2000; Yin and Harrison, 2000) and is thus the oldest tectonic structure in the investigation area. It separates the Tethyan Himalaya in the south from the Lhasa terrane in the north. In the investigation area the Tethyan Himalaya is composed of Late Precambrian to Lower Paleozoic sedimentary and metasedimentary rocks and Permian to Upper Cretaceous sedimentary rocks as well as an ophiolitic mélange sequence, while the Gangdese (or Mount Kailas) Range forms the southern flank of the Lhasa terrane and is composed of Cretaceous—Lower Tertiary intrusive and volcanic
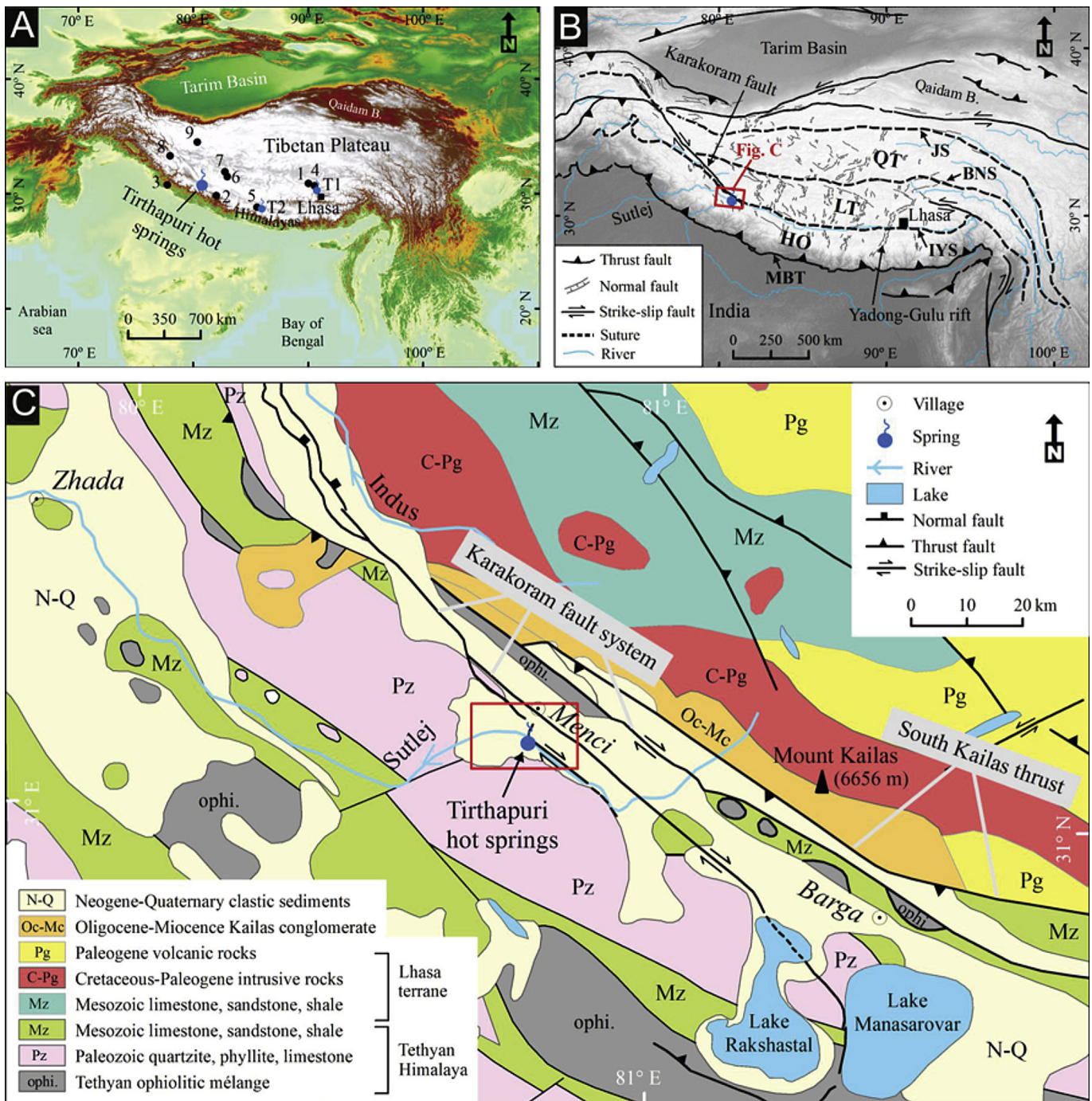
Fig. 1. (A) Overview map of High Asia with location of Tirthapuri hot springs. Black dots indicate the locations of paleoclimatic proxy records mentioned in the text: 1 — Tianmen Cave, Cai et al. (2010, 2012); 2 — Timta Cave, Sinha et al. (2005); 3 — Bittoo Cave, Kathayat et al. (2016); 4 — Nam Co, Zhu et al. (2015); 5 — Paiku Co, Wünnemann et al. (2015); 6 — Ngangla Ring Tso, Hudson et al. (2015); 7 — Baqan Tso, Huth et al. (2015); 8 — Tso Kar, Demske et al. (2009); 9 — Sumxi Co, Van Campo and Gasse (1993). Travertine sites mentioned in the text: T1 — Chusang travertine, Wang et al. (2016); T2 — Nyalam travertine, Zentmyer et al. (2008). (B) Generalized tectonic overview map of the Himalaya–Tibetan orogen showing major tectonic units (modified after Yin and Harrison, 2000; Blisniuk et al., 2001). IYS: Indus - Yarlung Tsangpo suture; BNS: Bangong - Nujiang suture; JS: Jinsha suture; MBT: Main boundary thrust; HO: Himalaya Oregon; LT: Lhasa terrane; QT: Qiangtang terrane. (C) Geological map of the Menci basin and the wider Tirthapuri region (marked as a red square and shown in Fig. 2; modified after Murphy et al., 2000; Murphy et al., 2000; Murphy and Yin, 2003; CIGMR, 2004). The IYS separates the Tethyan Himalaya from the Lhasa terrane and roughly follows the NW-SE trending axis of the Barga and Menci basins and the Indus River further to the northwest. (For interpretation of the references to colour in this figure legend, the reader is referred to the web version of this article.)

rocks (Gangdese batholith and magmatic arc; Fig. 1C; Yin et al., 1999; CIGMR, 2004; Murphy and Yin, 2003). The >2.5 km-thick Kailas conglomerate, which is a molasse sediment that formed during the Late Oligocene—early Miocene, rests unconformably on the Gangdese batholith (Fig. 1C; Aitchison et al., 2002; DeCelles

et al., 2011). Furthermore, the IYS has been overprinted by potentially multiple younger tectonic events; the IYS is strongly modified by a series of moderate-to-high-angle south-dipping reverse faults (an orogen-scale fault system known as Great Counter thrust) that were interpreted together with north-dipping shortening

structures in the Tethyan Himalaya as a large-scale "pop-up" structure that formed during the late Tertiary (Searle et al., 1990, 1997; Hodges, 2000). The trace of the Great Counter thrust runs along the northern margin of the Menci and the Barga basins and is regionally known as the South Kailas thrust (Fig. 1C; Yin et al., 1999; Murphy and Yin, 2003; DeCelles et al., 2011).

Tectonically, the Menci basin is bound to the Karakoram fault system (KFS; Fig. 1C). The NW-SE-trending KFS extends from the Pamir to the Pulan graben system in southern Tibet. It is an important active right-lateral strike-slip fault in western Tibet and partly overprints the IYS (Hodges, 2000; Yin and Harrison, 2000). The kinematics, geometry and chronology of the KFS are still under debate and the KFS is variably inferred as (i) being the result of eastward extrusion of northern Tibet (Armijo et al., 1986, 1989), (ii) oblique convergence between India and Tibet (McCaffrey and Nabelek, 1998), or (iii) may be explained as an accommodation zone that transfers east-west extension from more widely-spaced rifts in the south to the more closely-spaced rifts in the north (Yin, 2000). Fault activity along the KFS dates back to at least ca. 17 Ma, but for the development of the Menci and other pull-apart basins along the KFS the transtensional fault activity that commenced ca. 11 Ma ago and continues until today is most relevant (Rumelhart et al., 1999; Murphy et al., 2000). It is estimated that during that time approximately ~60–100 km of right-lateral offset were accommodated along the southern segment of the KFS, i.e. the fault segment that also controls the interconnected Zhada, Menci and Barga basins (Fig. 1C; Murphy et al., 2000; Wang et al., 2008a; Saylor et al., 2010a).

A sedimentological study by Wang et al. (2008a) suggests that the Zhada basin is filled with up to ~800 m of clastic sediments that can be divided into a basal fluvial unit (~0–220 m), an intermediate lacustrine unit (~220–610 m) and an interbedded lacustrine-fluvial unit (~610–800 m). Similar sedimentological findings were reported by Kempf et al. (2009) and Saylor et al. (2009; 2010a,b) for the Zhada basin and by Li et al. (1983) and Wang et al. (2008a) for the Menci basin. Biostratigraphic and magnetostratigraphic data suggest that these basins were filled during the Late Neogene until the Early Pleistocene (i.e. ca. 9 to <1 Ma; Meng et al., 2008; Wang et al., 2008b; Saylor et al., 2009; Li et al., 2011). In the Menci basin these fluvial and lacustrine sediments are tectonically tilted to the northeast by ~8–12° (Wang et al., 2008a).

3. Methods

Field investigations involved sedimentary logging and geomorphological field mapping, the latter was aided by analysis of Google Earth imagery and the 30 m resolution digital elevation model (DEM) derived from the Shuttle Radar Topography Mission (SRTM). Valley cross-sections were constructed based on the SRTM data and via elevation measurements obtained in the field using a hand-held Global Positioning System (GPS). Additionally, river and terrace long profiles were derived from ALOS AW3D30 data (Tadono et al., 2014).

Travertine blocks were collected from individual travertine deposits capping the fluvial terraces in the Tirthapuri hot spring area. All travertine samples were halved and thin sections were made for 16 samples with representative crystal fabrics. The microscopic travertine fabrics were examined under a Nikon Eclipse E400POL microscope using transmitted-light. Sub-samples were obtained for each travertine sample for powder X-ray diffraction (XRD) analyses and scanning electron microscope (SEM) analyses were performed on selected polished slabs (using a JEOL JSM-6010LV).

For ^{230}Th/U dating dense and clean travertines with primary fabrics were sub-sampled using a hand-held drill and a tungsten carbide drill bit. Chemical separation and purification of U and Th

isotopes followed a modified protocol described in Hoffmann (2008) and Hoffmann et al. (2016). U and Th isotope measurements were undertaken using a ThermoFinnigan Neptune Multi-Collector Inductively Coupled Plasma Mass Spectrometer (MC-ICP-MS) following procedures outlined in Hoffmann et al. (2007). All ages were calculated using the half-lives reported in Cheng et al. (2000) (λ234 and λ230). A ^{238}U/^{232}Th activity ratio of 0.8 $\pm$ 0.4 was used to correct the detrital ^{230}Th contamination (Wedepohl, 1995). For travertine samples with high detrital ^{232}Th, Osmond type isochron ages were calculated based on the measured activity ratios of 3–5 subsamples from the same depositional layer.

For OSL dating (Huntley et al., 1985; Rhodes, 2011) standard preparation techniques were used to isolate quartz grains from the bulk sediment samples (Wintle, 1997; Gliganic et al., 2015). Single quartz grains were stimulated with green (532 nm) laser light (Bøtter-Jensen et al., 2003) for 2 s at 125 °C in a Risø DA20 TL/OSL reader and the ultraviolet OSL emissions were measured using an Electron Tubes Ltd 9635Q photomultiplier tube fitted with a 7.5 mm Hoya U-340 filter. Laboratory irradiations were given using a calibrated ^{90}Sr/^{90}Y beta source mounted on the Risø TL/OSL reader. The single-aliquot regenerative dose (SAR) procedure (Murray and Wintle, 2000) was used to estimate equivalent dose (De) values. Regenerative dose preheats (10 s) and test dose preheats (5 s) of 220 °C were used. The appropriateness of the SAR procedure was assessed using standard tests including a recycling ratio test, recuperation test (Murray and Wintle, 2000), OSL-IR depletion ratio (Duller, 2003), and dose recovery tests (Roberts et al., 1999; Murray and Wintle, 2003). The central age model (CAM; Galbraith et al., 1999) and minimum age model (MAM; Galbraith et al., 1999) were used to investigate De distributions and determine representative De values. The total environmental dose rate for each sample (Table 1) was estimated using standard techniques (a combination of beta counting using a GM-25-5 beta counter (Bøtter-Jensen and Mejdahl, 1988) and thick-source alpha counting) and the conversion factors of Guérin et al. (2011) to calculate beta and gamma dose rates. The cosmic-ray dose rate was calculated following Prescott and Hutton (1994) and an internal alpha dose rate of 0.03 $\pm$ 0.01 Gy/ka was assumed.

4. Results

4.1. Fluvial terraces and alluvial fans

The Sutlej River and its tributaries have incised deeply into the Late Neogene to Early Pleistocene basin infill of the central Menci basin and have partly reached bedrock (Figs. 2 and 3). At least 4 main terrace levels can be identified on the SRTM based DEM and are labelled (from younger to older) as T1 to T4 and range in altitude from ~4360 m asl. (T1) to ~4600 m asl. (T4; Figs. 2–4). Furthermore, remnants of a paleosurface can be identified at ~4650 m asl. According to an unpublished geological map of the Geological Survey of Southern Tibet this paleosurface is underlain by the Xiangzi formation (Fig. 2), which is Early Pleistocene in age (Meng et al., 2008). The main terrace levels T1 to T4 can be semi-continuously traced along the Sutlej River and its tributaries (in some instances for ~5–6 km) and tread widths vary from ~100 m to ~1.5 km (Figs. 2 and 3). The heights of individual terrace risers are ~8 m (T1), ~20 m (T2), ~65 m (T3) and ~155 m (T4), respectively (Figs. 2 and 3).

Field mapping and Google Earth imagery further reveal that (i) these terraces preserve a veneer of younger fluvial gravels typically ~0.5 to 2–3 m in thickness that is separated from the basin infill via an angular unconformity or disconformity (Fig. 5B and C); (ii) they are partly unpaired and (iii) in addition to the main terrace levels several sub-levels can be discerned (Figs. 3 and 4). We use longitudinal and valley cross-profiles of the Sutlej River as well as

Table 1
Sample dose rate, De, and age data for OSL samples from Tirthapuri. Uncertainties are reported at the 68% confidence level. Samples TP-OSL-9 to 12 were taken from various positions along a road cut at ca. 80°44′33″ E, 31°08′37″ N, between 4390 and 4395 m asl. The sampling coordinates for TP-T-12 are 80°45′19″ E, 31°07′35″ N, 4380 m asl. Note that samples TP-OSL-9 to 12 are from an alluvial fan (Fig. 4C), while sample TP-T-12 is from fluvial sediments cemented by travertine (Fig. 4B).

| Sample	Sample depth (cm)	Dose rate data (Gy/ka)				Dose-recovery data		De data				
		Gamma dose rate	Beta dose rate	Cosmic dose rate	Total dose rate[a]	Measured /Given ratio	OD	CAM De (Gy)	OD	MAM De (Gy)	MAM age (ka)
TP-OSL-9	116	1.25 ± 0.03	2.23 ± 0.12	0.35 ± 0.03	3.85 ± 0.19			60.8 ± 3.5	46 ± 5	35.9 ± 4.4	9.3 ± 1.2
TP-OSL-10	230	1.35 ± 0.03	2.30 ± 0.12	0.30 ± 0.03	3.98 ± 0.20	1.01 ± 0.04	0	58.9 ± 3.5	26 ± 6	43.3 ± 5.4	10.9 ± 1.5
TP-OSL-11	365	1.43 ± 0.04	2.30 ± 0.13	0.26 ± 0.03	4.01 ± 0.20			65.2 ± 4.5	42 ± 6	37.1 ± 4.9	9.3 ± 1.3
TP-OSL-12	620	1.40 ± 0.04	2.25 ± 0.15	0.19 ± 0.02	3.87 ± 0.22	1.04 ± 0.04	0	53.0 ± 4.2	48 ± 7	28.5 ± 4.9	7.3 ± 1.3
TP-T-12	150	0.58 ± 0.02	0.88 ± 0.05	0.37 ± 0.04	1.86 ± 0.10	0.97 ± 0.05	11	33.7 ± 1.5	31 ± 5	25.3 ± 2.87	13.6 ± 1.7

[a] Includes and internal dose rate of 0.03 ± 0.01 Gy/ka.
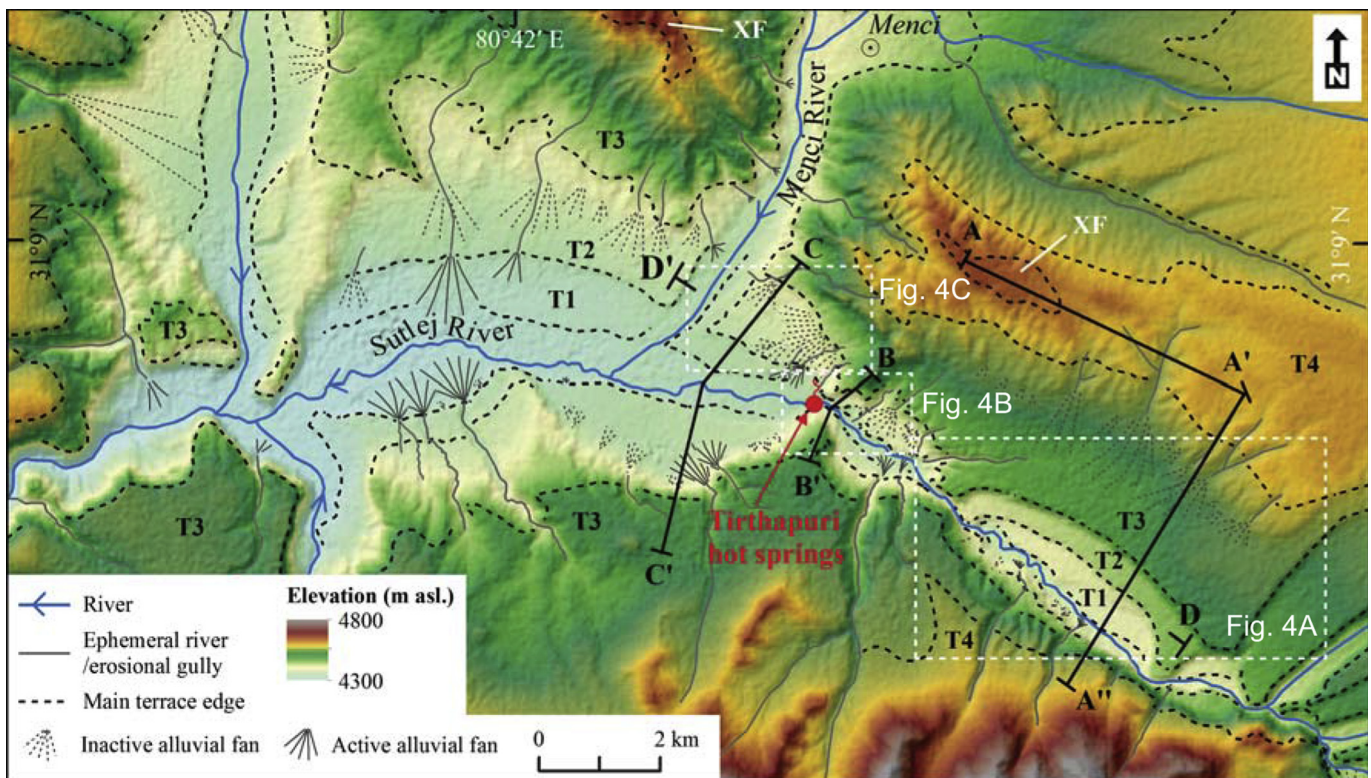
Fig. 2. DEM based on SRTM 1 arc (30 m) data for the central Menci basin with major fluvial terraces highlighted. At ~4650 m asl. a paleosurface is preserved (dashed line, no terrace label) that is underlain by the Early Pleistocene Xiangzi Formation (XF).

geomorphological mapping criteria to group these main and sub-terraces into terrace generations. The main terrace levels are all characterized by particularly wide treads (≥100 m) and separated from each other by terrace risers that are ≥8 m high (Figs. 2 and 3). Well-preserved paleo-channels of a former braided river network are present on the treads of T1 and T2 (and their sub-terraces), while no such paleochannels are discernable at any of the higher terrace generations anymore due to a cover of alluvial fans and eolian deposits and the presence of relatively thick soil (Fig. 4). Furthermore, T2 terraces show slightly more alluvial and eolian cover compared to any of the T1 terraces, where such sediments are almost completely lacking (Fig. 4). In addition the edges of all terraces belonging to the T1 generation are sharp and geomorphologically fresh while the terrace edges of the T2 generation show incipient gullying (of a few meters; Fig. 4A). Erosional gullies several hundred meters in length are frequent for the edges of the T3 generation and some of these gullies have advanced into 1–2 km

long ephemeral streams that deeply incise into the treads of the T4 terraces and sub-terraces, respectively (Figs. 2 and 4A). The resulting terrace generations (labelled as T1 to T4) and their sub-terraces (labelled with a positive or negative exponent according to their genetic position above or below the respective main terrace) are indicated in the Figs. 3–6.
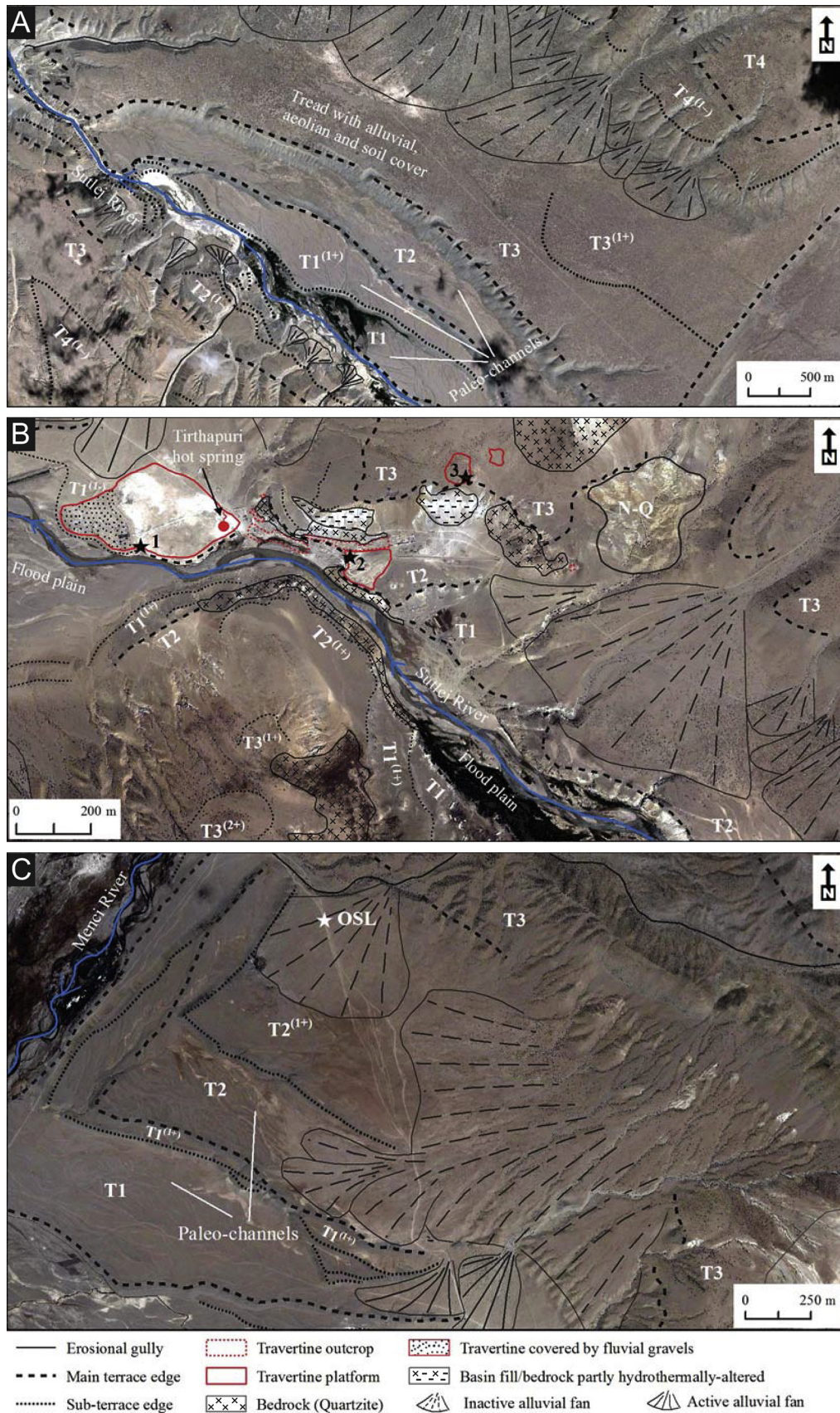
In the immediate vicinity of the hot springs the valley narrows and the Sutlej river partly incises into bedrock and several of the terraces (particularly the T2 terraces along the southern river bank) are thus developed as strath terraces (Figs. 4B and 5C).

In addition to these fluvial terraces and travertine deposits several generations of alluvial fans that originate from the adjacent risers of older terraces, hill slopes or tributaries can be observed in the central Menci basin. These alluvial fans are adjusted to different terrace levels; i.e. most of the active fans run out in the modern floodplain or on one of the wide treads of the T1 terrace generation, while alluvial fans adjusted to higher terraces and disconnected
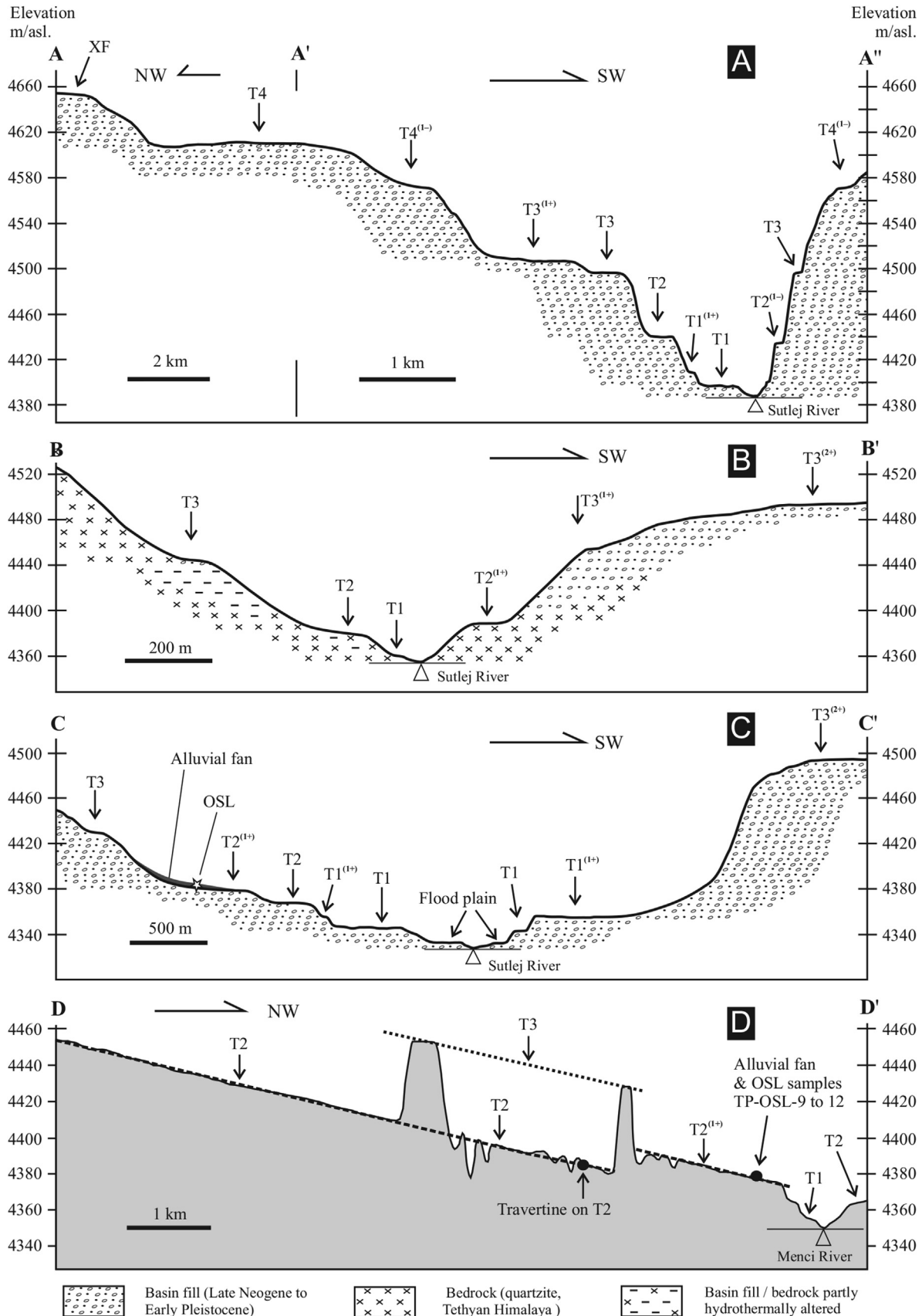
Fig. 3. Simplified cross- and longitudinal profiles of the Sutlej River valley showing the main terraces and their sub-terraces (see Fig. 2 for location of profile sections). (A) Profile section A-A'-A″ starts at the paleosurface preserved in the central Menci basin (underlain by the Early Pleistocene Xiangzi Formation (XF)) and traverses the entire set of terrace generations. (B) Profile section B-B' is located next to the Tirthapuri hot springs where several terraces are developed as strath terraces. (C) Profile section C-C' also traverses a fossil alluvial fan that was deposited on terrace T2^(1+) and has been sampled for OSL dating. (D) Longitudinal profile section D-D' along the Sutlej River showing the gradient of the terraces T2, T2^(1+) and T3. The current level of the Sutlej River is 4352 m asl. at Tirthapuri.

Fig. 4. Geomorphology of the investigation area (base maps from Google Earth; see Fig. 2 for location of each map). (A) Terrace treads T1 to T4 and erosional and depositional surface features. (B) Geomorphology in the immediate vicinity of the Tirthapuri hot springs. Note travertine platforms T1, T2 and T3. Numbered stars indicate locations of travertine samples taken for [230]Th/U (or OSL) dating: 1 − sample TP-T-1; 2 − samples TP-T-10, TP-T-12 (OSL), TP-T-15 and TP-T-16; 3 − sample TP-T-6. N-Q: Late Neogene to Early Pleistocene fluvio-lacustrine sediments (i.e. basin infill). (C) Terraces immediately northwest of the Tirthapuri hot springs are covered by several generations of alluvial fans. The star indicates the approximate location of four OSL samples taken from an alluvial fan that is deposited on terrace T2[(1+)].
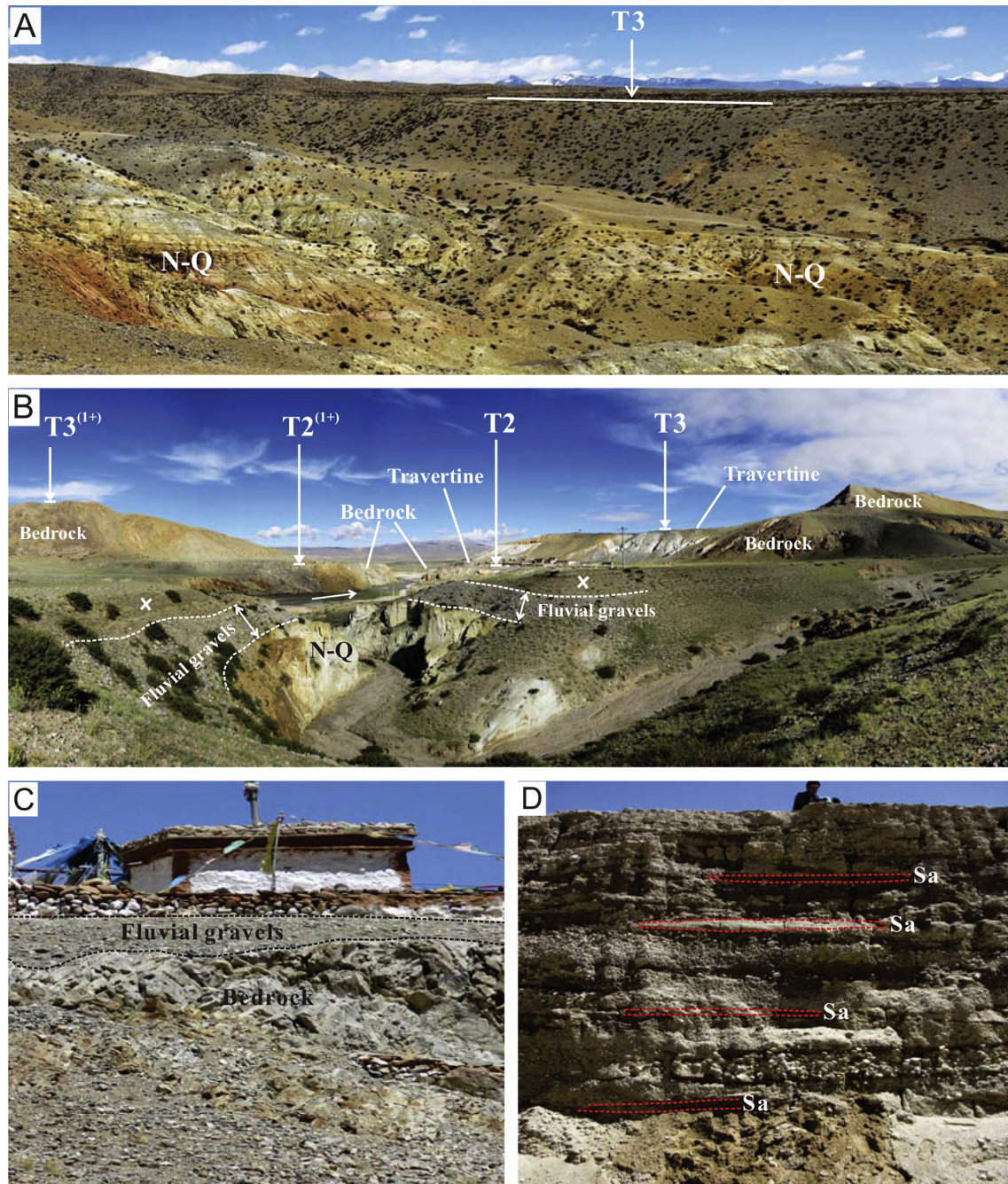
Fig. 5. (A) View over the central Menci basin towards northeast. Note the extensive tread of terrace T3 and the slightly tilted Late Neogene to Early Pleistocene strata (N-Q) that make up the basin infill. (B) Field photo showing the terraces upstream of the Tirthapuri hot springs. View towards west. Note the ~1–2 m thick layer of fluvial gravels belonging to terrace T2 and overlying the basin infill (N-Q) and alluvial fan sediments (marked with a X) atop these gravels. (C) Outcrop in terrace T2 showing a ~0.5 m thick layer of fluvial gravels resting on bedrock. (D) Outcrop in an alluvial fan that was deposited on the T2$^{(1+)}$ terrace ~2 km northwest of the Tirthapuri hot springs. The OSL samples TP-OSL-9 to TP-OSL-12 were taken from four different sand lenses (Sa) that are intercalated into this otherwise coarse-grained deposit. Note that the sand lenses from which the OSL samples were obtained are laterally separated from each other by several tens of meters.

from the floodplain are common too (Figs. 2 and 4). One such fossil fan is situated ~2 km northwest of the hot spring area and was deposited on top of terrace T2$^{(1+)}$ (Fig. 4C). The fan is ~8° steep at its former apex and ~3–4° in its distal parts. Exposures along a road that cuts through the distal part of the fan reveal gravelly lenses with a sand matrix that are up to ~50 cm thick and extend laterally for ≥10 m before pinching out. These gravel lenses are poorly sorted, clast and sometimes matrix supported and often show

inverse grading and sharp basal contacts, suggestive of cohesive to cohesionless mass flow mechanism (Fig. 5D). Well sorted sand lenses ~10–30 cm in thickness are interbedded into these alluvial fan sediments and four OSL samples (TP-OSL-9 to 12) that are spaced ~15 m from each other and vertically cover the entire sedimentary sequence were obtained from such lenses for OSL dating (Fig. 5D).
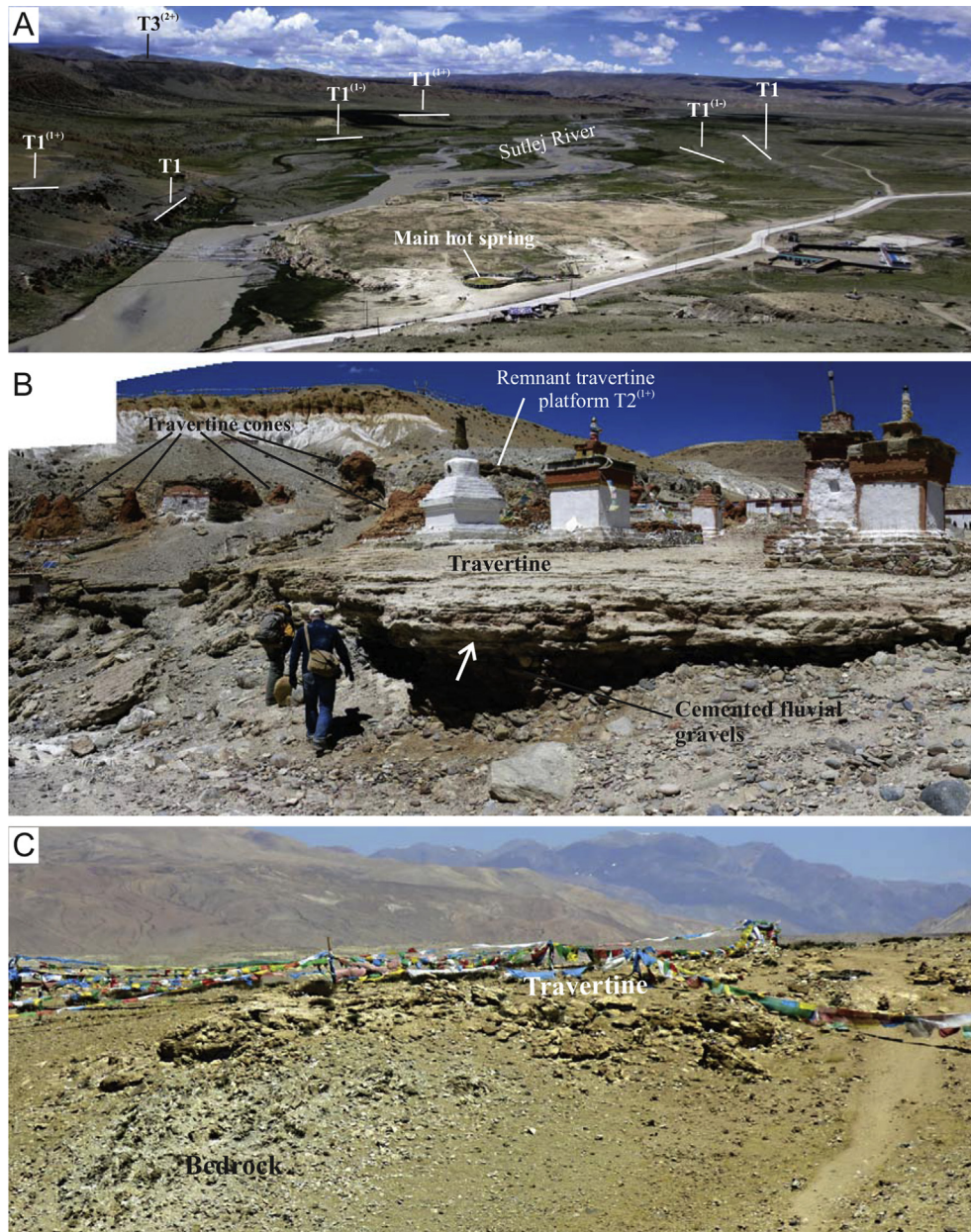
Fig. 6. (A) Image (view towards southwest) showing the travertine platform T1 and the modern hot springs as well as the fluvial terraces belonging to the T1 generation. (B) Image (view towards north) showing the travertine platform T2. Fluvial gravels are underlying this platform and are partly cemented by hydrothermal carbonate, but layers of fluvial sediment are also partly intercalated into the bedded travertine platform (arrows). Note the travertine cones and the remnant travertine platform T2$^{(1+)}$ in the background. (C) The highly weathered travertine platform T3 atop of terrace T3. View towards north.
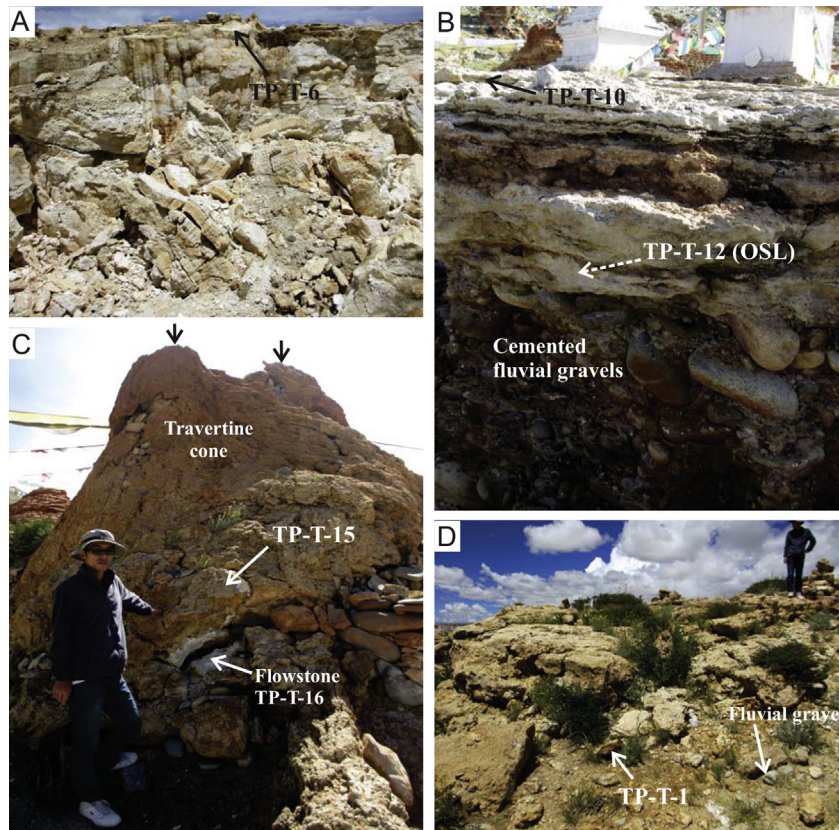
4.2. Travertine platforms

An extensive travertine deposit that is interbedded with fluvial gravels occurs in the modern floodplain of the Sutlej River and mapping in the hot spring area revealed that the treads of the terraces T2 and T3 are partly covered by thick sheets of travertine as well (Figs. 4B and 6). Because these carbonate deposits have a higher resistance to erosion compared to the underlying unconsolidated fluvial sediment they slightly stick out of the landscape, hence the term travertine platform is used to refer to these hydrothermal carbonate deposits that are found on multiple terrace treads.

The lowest travertine platform is situated adjacent to the Sutlej River at an altitude of ~4360 m asl (Figs. 4B and 6A). This platform

has a size of 8.1×10^4 m^2, is slightly convex, has a maximum thickness of ~8 m with its base being situated at the level of the Sutlej River (~4352 m asl.), and is composed of white to light-brownish carbonate (Figs. 6A and 7A). Active and fossil travertine pools can be observed on this platform and the main hot spring is situated on top of it (Fig. 6A). Layers of fluvial gravels up to ~20–30 cm in thickness are occasionally intercalated into this travertine deposit. The surface of the platform is at the same altitude as the T1 terrace and we thus refer to this platform as T1 travertine platform. The distal parts of this platform (i.e. ~260 m downstream from the main hot spring) are terraced and slightly lower in elevation and overlain by fluvial gravels. This lower part of the T1 travertine platform can be topographically correlated with terrace T1$^{(1-)}$ (Figs. 4B and 6A).

Fig. 7. (A) Outcrop in the travertine platform T1 and position of travertine sample TP-T-6. (B) Outcrop in travertine platform T2 showing bedded travertine directly overlying fluvial gravels. The fluvial sediment is cemented by the hydrothermal carbonate. Note that fluvial gravels and sands are also intercalated into the travertine (arrows). Samples TP-T-10 and TP-T-12 (approximate location indicated) were taken for [230]Th/U and OSL dating, respectively. (C) Image showing a travertine cone that accumulated on the T2 travertine platform and has been sampled for [230]Th/U. Note the white flowstone that precipitated in a small cavity inside the cone. (D) Image showing that the remnants of travertine platform T3. Note the position of [230]Th/U sample TP-T-1 and the fluvial gravels that are capped by travertine.

Further travertine deposits occur between ~4380 and 4390 m asl., just ~360 m further to the east of the modern hot springs (Figs. 4B and 6A). Most prominent is a travertine platform at ~4380 m asl. that correlates in altitude with the terrace T2 (thus termed T2 travertine platform) and has an areal extent of ~9.8 × 10³ m² with at least 4 travertine cones built on top of it. These travertine cones indicate the position of paleo-spring orifices and are ~2–4 m high and have a bottom diameter of ~1–5 m (Fig. 7C). The natural coloring of these cones as well as of the travertine that makes up the platform is brown, but most cones were painted red by the local people (Fig. 7C). Outcrops along the Sutlej River reveal that (i) the travertine platform is composed of horizontal sheets of travertine with internal dm-scale bedding and can attain a total thickness of ~3 m (Figs. 6B and 7B); (ii) towards the base of the platform fluvial sediments are occasionally inter-bedded with travertine, while the upper ~2.5 m lack such an interbedding; and (iii) the travertine platform overlies fluvial gravels and sands that are partly cemented by the hydrothermal carbonate (Figs. 6B and 7B). Remnants of a higher travertine plat-form at ~4390 m asl. that correlates with the T2$^{(1+)}$ terrace level are preserved at the bedrock slope along the northern margin of the T2 travertine platform (Figs. 4B and 6B). More travertine cones emerge from faults and fractures along this bedrock slope and correlate in altitude with this remnant travertine platform and the T2$^{(1+)}$ terrace level (Fig. 6B).

Further travertine occurrences are preserved ~660 m northeast of the main hot spring (Fig. 4B). There remnant travertine deposits cover a ~9.8 × 10³ m² large area of terrace T3 at ~4445 m asl. and a

~1.3 × 10³ m² large area at ~4460 m asl. The altitude of this latter travertine deposit coincides with the level of terrace T3$^{(1+)}$. Both travertine deposits are horizontally layered, brownish in color, reveal internal bedding on the cm-scale and are partly covering bedrock and partly fluvial gravels (Fig. 7D). No travertine cones are associated with these heavily eroded travertine occurrences and we refer to these deposits as travertine platforms T3 and T3$^{(1+)}$, respectively.

4.3. Travertine fabrics

The travertine fabrics of each travertine platform were investi-gated in order to identify suitable (i.e. primary) fabrics for [230]Th/U dating. The macro- and micro-fabrics that characterize the lith-ofacies of each travertine platform are outlined in the following and summarized in Table 2.

Travertine samples from the travertine platform T1 show well-developed mm-scale lamination composed of alternating brown and relatively thinner white laminae. Transmitted light microscopy reveals that the brown laminae consist of fan-like aggregates (made of aragonite needle crystals as confirmed by XRD analysis), while the thin white laminae consist of micrite (Fig. 8A). SEM images further reveal that (i) micrite commonly precipitates at the surface of aragonitic fans filling the space between aragonitic needles and (ii) calcified algal filaments are present among the aragonitic nee-dles as well (Fig. 8B).

Samples from the travertine platform T2 and from the travertine cones built on top of this platform are dominated by a porous

Table 2
Summary of travertine lithofacies at Tirthapuri.

Lithofacies	Distribution	Fabrics	Porosity	Interpretation	Depositional environment
Laminated travertine	Travertine platform T1	*Aragonite*: crystals ~0.1–0.5 mm long, forming fans or small spherulites; Under SEM: *microbial and algal filaments* discernable; *Lamination*: aragonitic laminae (~1 –10 mm) alternating with micritic laminae (≤0.5 mm); aragonitic laminae show sub-laminae (~0.25 mm)	<5 vol%; *intercrystalline pores* (0.02–0.1 mm)	*Aragonite*: precipitated by hydrothermal water >40–45 °C and/or a Mg/Ca ratio of >1.1; microbially mediated calcite precipitation likely (Guo and Riding, 1992; Folk, 1994; Pentecost, 2005); *Lamination*: due to cyclic (e.g. seasonal, monthly or even daily) changes in water temperature or flow velocity (impacting on the Mg/Ca ratio), and/or temperature related variations of microbial activity (Guo and Riding, 1992; Folk, 1994)	Sheet flow over flat terrain or in shallow pools (Chafetz and Folk, 1984; Guo and Riding, 1992)
Layered travertine	Travertine platform T2	*Dendrites* (made of calcite) up to 10 mm long, forming crystalline fans, partly recrystallized into a mosaic of coarse-grained or bladed sparites; *Clotted peloidal micrite* with organic mucilage and filaments; *Layering*: ~5–15 mm thick dendritic layers alternating with ~1–2 mm layers of clotted peloidal micrite; Sometimes sub-rounded to angular *detrital grains* (~0.05–0.6 mm)	20-30 vol%; *gas bubbles* (mm to cm); *microbial moulds* (0.5–1 mm); *inter-dendritic pores* (0.1–0.5 mm)	*Dendrites*: deposited by highly supersaturated hydrothermal water via rapid CO_2 degassing (fast abiotic calcite precipitation; Jones et al., 2005); *Clotted/peloidal micrite*: microbially mediated calcite precipitation; *Layering*: due to cyclic (e.g. seasonal) changes in water temperature or flow velocity (Jones and Renaut, 2008); bacterial influence also possible (Della Porta, 2015); *Detrital gains*: short transport distances, mainly fluvial in origin	Fast flow over smooth slopes or steep travertine cones; partly also on flat ground between cones (Rainey and Jones, 2009; Gandin and Capezzuoli et al., 2014)
Lime-mudstone	Travertine platform T3	Mostly structureless *micrite and microsparite* (made of calcite) and *fan-like and botryoid-shaped crystals* recrystallized into sparite *Faint lamination* made of micro-layers of botryoid-shaped crystals alternating with micrite (0.2–0.05 mm); *Intercalated detrital horizons* (~10 –20 mm thick) rich in sub-rounded to sub-angular detrital sand sized grains	<2–3 vol %; *intercrystalline pores* (0.2–0.05 mm)	*Massive micrite*: strong similarities to mud-limestone deposited in slightly supersaturated, stagnant water, either microbially-induced (Pedley, 1990) or abiotically-controlled due to evaporation (Pentecost, 2005); *Botryoid-shaped crystals and lamination*: relics of hydrothermal precipitation; *Microsparite and sparite*: recrystallization (aggradational neomorphism; Love and Chafetz, 1988); *Detrital horizons*: repeated influx of fluvial grains, short transport (Sant'Anna et al., 2004)	Low-energy stagnant water like ponds or marshes partly fed by hydrothermal water, repeated influx of meteoric (fluvial) water (Pedley, 1990)
Flowstone	Cavity inside travertine cone	*Lamination*: 0.5–1 mm thick palisade columnar sparitic laminae alternate with very thin micritic laminae (made of calcite).	0 vol%	Abiotically precipitated by percolation water with relatively low but constant supersaturation (Frisia et al., 2000). Stable oxygen and carbon isotopes suggest hydrothermal origin.	Travertine fissures or cavities, via re-infiltration of hydrothermal water.

layered travertine lithofacies. The layering is caused by cm-thick bands of wavy but laterally continuous dendritic crystals composed of low-Mg calcite (partly recrystallized into sparites), that alternate with mm-thick bands of clotted/peloidal micrite, as revealed by transmitted light microscopy and XRD analysis (Fig. 8C and D). Pores such as coated bubbles (≤1 cm) and microbial moulds (≤1 mm in size; Fig. 8D) give this layered travertine lithofacies a porous character. Detrital sand-sized grains of various lithology and showing a sub-rounded to angular grain morphology are common, particularly in the basal section of the platform (Figs. 7B and 8E). The flowstone-like sample from the cavity inside a travertine cone that grew on the travertine platform T2 is dense and clean and composed of laminated calcite that consists of ~0.5–1 mm thick laminae of palisade columnar sparite alternating very thin micrite laminae (Fig. 8F).
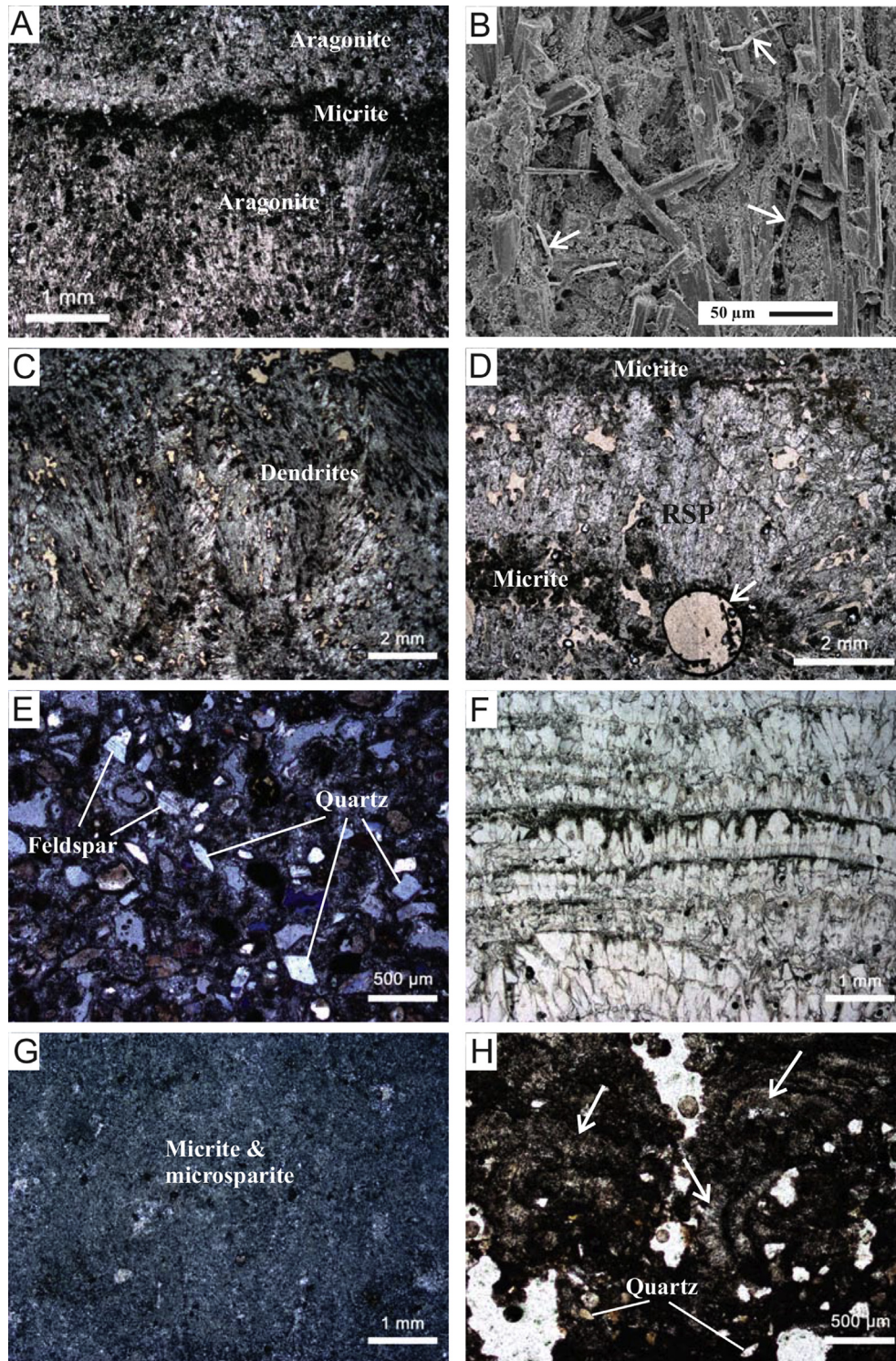
Samples from the travertine platform T3 have very low porosity and are composed of massive structureless micrite and micro-sparite resembling a mud-limestone lithofacies (Fig. 8G). Locally remnant layers of fan-like and botryoid-shaped crystals that are recrystallized into sparite and alternate with micritic layers are preserved too (Fig. 8H). In some samples from the T3 platform

~1–2 cm thick bands composed of micrite that is rich in sand-sized grains of detrital origin are intercalated into the otherwise clean mud-limestone lithofacies.

4.4. ^{230}Th/U dating results

Based on the petrographic analyses, we targeted the aragonite fabric in sample TP-T-6 (travertine platform T1; Fig. 7A), the dendrite fabric in samples TP-T-10 and TP-T-15 (travertine platform T2; Fig. 7B and C) and the micritic/microsparitic fabric in sample TP-T-1 (travertine platform T3; Fig. 7D) as well as the palisade columnar sparite of the flowstone (sample TP-T-16, travertine platform T2; Fig. 7C) for ^{230}Th/U dating. A total of 14 sub-samples were analyzed for ^{230}Th/U age determinations, including sub-samples from the same depositional layer for some samples to check for age reproducibility and an eventual isochron dating approach (Table 3).

Three subsamples of sample TP-T-6 yield consistent ^{232}Th-corrected ages (weighted mean of 0.22 ± 0.03 ka; Table 3). Due to the high detrital ^{230}Th contamination the ^{232}Th-correction is failing and no age can be derived for sample TP-T-10. Three subsamples

Fig. 8. Photomicrographs of representative microfabrics from the travertine platforms T1, T2 and T3. (A) Sample TP-T-6 from the travertine platform T1 showing well-developed lamination that is composed of mm-thick laminae of aragonitic needle crystals alternating with very thin micritic laminae. (B) SEM image of micrite (sample TP-T-6) showing calcified microbial or algal filaments (arrows). (C) Sample TP-T-15 is characterized by large dendritic crystals. (D) The dendritic crystals of sample TP-T-15 are partly recrystallized into sparite and form cm-thick layers that alternate with mm-thin layers of clotted/peloidal micrite. Note the circular microbial mould (arrow) within the clotted/peloidal micritic lamina. (E) Cemented fluvial sands from the base of travertine platform T2 (Sample TP-T-12) showing numerous angular to sub-rounded sand-sized grains of various lithology. (F) The flowstone sample TP-T-16 from a cavity inside a travertine cone is composed of ~0.5–1 mm-thick palisade columnar sparitic laminae alternating with very thin micrite laminae. (G) Sample TP-T-1 from the travertine platform T3 is composed of massive micrite and microsparite. (H) Fan-like crystals that are sometimes recrystallized into sparite (arrows) and are arranged in a botryoid-like fabric are present in some samples from the T3 travertine platform. Angular to subrounded sand-sized detrital grains (e.g. quartz) are sometimes present within a calcite matrix. Images E and H taken in cross-polarized light, all other images taken in plane-polarized light.

Table 3

Uranium and thorium concentrations, activity ratios and uncorrected and corrected ^{230}Th/U ages for the Tirthapuri travertine. Correction for detrital contamination for individual subsamples assumed a value of 0.8 ± 0.4 for the ^{238}U/^{232}Th activity ratio of the detrital component (Wedepohl, 1995). Isochron ages were calculated via Osmond-type isochron plot based on the measured activity ratios of 3—5 subsamples from each travertine sample. Ages are reported as time before chemical separation (AD 2014). Uncertainties are reported at the 95% confidence level. The sample coordinates are: TP-T-6 (80°44′59″E, 31°07′36″N, 4360 m asl.), TP-T-10, 12 and 16 (80°45′19″E, 31°07′35″N, 4380 m asl.), sample TP-T-1 (80°45′31″E, 31°07′42″N, 4445 m asl.).

Sample	^{238}U (ng/g)	^{232}Th (ng/g)	[^{230}Th/^{232}Th] activity ratio	[^{232}Th/^{238}U] activity ratio	[^{230}Th/^{238}U] activity ratio	[^{234}U/^{238}U] activity ratio	Age (ka) uncorrected	Age (ka) corrected	[^{234}U/^{238}U]$_{initial}$ activity ratio
TP-T-6 (subsamples from three adjacent depositional layers)									
TP-T-6a	323.8 ± 6.9	2.072 ± 0.048	4.47 ± 0.38	0.002 ± 0.000	0.009 ± 0.001	3.855 ± 0.008	0.27 ± 0.02	0.22 ± 0.03	3.861 ± 0.008
TP-T-6b	363.0 ± 6.7	2.685 ± 0.056	3.95 ± 0.30	0.002 ± 0.000	0.010 ± 0.001	3.858 ± 0.007	0.27 ± 0.02	0.22 ± 0.03	3.865 ± 0.008
TP-T-6c	341.3 ± 6.6	1.951 ± 0.044	4.74 ± 0.36	0.002 ± 0.000	0.009 ± 0.001	3.834 ± 0.007	0.25 ± 0.02	0.21 ± 0.03	3.840 ± 0.008
TP-T-10	178.5 ± 1.9	335.348 ± 3.667	0.64 ± 0.01	0.614 ± 0.002	0.396 ± 0.004	1.415 ± 0.007	35.29 ± 0.43	failed[b]	
TP-T-15 (subsamples from the same depositional layer)								10.0 ± 0.2[a]	3.64 ± 0.20
TP-T-15a	47.8 ± 1.0	18.311 ± 0.437	2.79 ± 0.11	0.125 ± 0.002	0.350 ± 0.014	3.503 ± 0.031	11.36 ± 0.48	8.25 ± 1.37	3.847 ± 0.160
TP-T-15b	51.4 ± 1.0	32.129 ± 0.814	1.82 ± 0.11	0.204 ± 0.003	0.372 ± 0.025	3.324 ± 0.015	12.79 ± 0.92	7.39 ± 2.48	3.837 ± 0.274
TP-T-15c	48.6 ± 1.0	12.645 ± 0.307	4.00 ± 0.30	0.085 ± 0.001	0.340 ± 0.026	3.462 ± 0.012	11.17 ± 0.89	9.04 ± 1.25	3.710 ± 0.098
TP-T-1 (subsamples from the same depositional layer)								127.5 ± 1.1[a]	3.93 ± 0.26
TP-T-1a	206.7 ± 5.1	44.574 ± 1.228	31.91 ± 0.16	0.071 ± 0.000	2.252 ± 0.013	2.927 ± 0.009	129.33 ± 1.37	127.68 ± 5.80	3.930 ± 0.060
TP-T-1b	253.4 ± 6.0	42.845 ± 0.923	39.57 ± 0.18	0.055 ± 0.000	2.189 ± 0.012	2.856 ± 0.007	128.80 ± 1.26	127.48 ± 4.46	3.784 ± 0.045
TP-T-1c	264.5 ± 5.4	76.319 ± 1.517	22.71 ± 0.10	0.094 ± 0.000	2.145 ± 0.010	2.782 ± 0.007	130.28 ± 1.19	127.95 ± 7.66	3.768 ± 0.077
TP-T-1d	339.8 ± 7.1	52.667 ± 1.018	45.06 ± 0.21	0.051 ± 0.000	2.285 ± 0.013	2.952 ± 0.007	130.47 ± 1.30	129.31 ± 4.27	3.932 ± 0.043
TP-T-1e	206.3 ± 4.4	28.866 ± 0.613	48.54 ± 0.23	0.046 ± 0.000	2.223 ± 0.012	2.904 ± 0.007	128.29 ± 1.26	127.22 ± 3.74	3.832 ± 0.038
TP-T-16 (subsamples a and b from top bottom of flowstone sample, respectively)									
TP-T-16a	61.6 ± 1.4	0.696 ± 0.083	78.18 ± 3.76	0.004 ± 0.000	0.289 ± 0.025	3.676 ± 0.013	8.85 ± 0.78	8.76 ± 0.78	3.752 ± 0.015
TP-T-16b	75.2 ± 2.0	1.753 ± 0.060	41.07 ± 1.40	0.008 ± 0.000	0.313 ± 0.013	3.581 ± 0.013	9.89 ± 0.41	9.71 ± 0.42	3.669 ± 0.016

[a] Ages are the Osmond-type isochron ages.
[b] The ^{232}Th correction failed due to high detrital contamination.

from the same depositional layer of sample TP-T-15 yielded ^{232}Th-corrected ages that overlap within error and the corresponding Osmond-type isochron age is 10.0 ± 0.2 ka (Table 3). The five subsamples from sample TP-T-1 gave ^{232}Th-corrected ages that also overlap within error (Table 3) with a weighted central mean of 127.9 ± 2.1 ka. Two subsamples from the bottom and the top of the flowstone sample TP-T-16 yielded ^{232}Th-corrected ages of 9.7 ± 0.4 ka and 8.8 ± 0.8 ka respectively (Table 3).

4.5. OSL dating results

Five sediment samples were collected for OSL dating: four from sand lenses in an alluvial fan overlying T2$^{(1+)}$ (TP-OSL-9 to −12; Fig. 5D) and cemented fluvial sands from immediately below the travertine platform T2 (TP-T-12; Fig. 7B). These sands partly fill the pores of underlying fluvial gravels, suggestive of sand deposition during the waning stage of a high discharge event followed by cementation of these sediments by hydrothermal carbonate.

Equivalent dose and dose rate data are shown in Table 1 and Fig. 9B and D. A typical OSL decay curve and dose-response curve are shown in Fig. 9A and C. Single-grain dose recovery results for all measured samples are statistically consistent with unity with overdispersion values between 0 and 11%, indicating that the SAR procedure can accurately estimate known radiation doses for these samples. Overdispersion values for De distributions range between 26% and 48%. The significant difference in overdispersion values between natural and dose-recovery datasets suggests that the natural De distributions of samples are affected by environmental factors such as beta-dose rate heterogeneity, partial bleaching, and/or post-depositional mixing. Given that all samples were transported and deposited in relatively high-energy fluvial or alluvial systems, partial bleaching is likely a significant factor affecting De distributions, suggesting that the MAM will best represent the burial dose (Galbraith et al., 1999).

The depositional age determined for TP-T-12 of 13.6 ± 1.7 ka represents the timing of fluvial activity immediately before commencement of travertine formation. Samples TP-OSL-9, -10, −11 and −12 were collected from sand lenses in an alluvial

fan overlying terrace T2$^{(1+)}$. The depositional ages of these four OSL samples range from 7.3 to 10.9 ka, albeit with relatively large errors on individual age estimates (e.g. 18% relative error for sample TP-OSL-12; 68% confidence level). Standard statistical homogeneity testing strongly suggests that these ages are consistent with a common value (95% confidence level; Galbraith, 2003), and we thus opted for calculating a weighted mean age of 9.1 ± 0.7 ka for the landform. The concordance of depositional ages for these four samples indicates that over ~6 m of alluvial sediments were deposited very quickly on top of terrace T2$^{(1+)}$ in the early Holocene.

5. Discussion

5.1. Interpretation of travertine fabrics

Detailed geochemical or petrographical analyses of the modern hot spring system are not available. Hence, for interpreting the travertine fabrics from the T1 to T3 terraces we limit ourselves to basic petrographic observations and interpretations based on comparisons with other hot spring carbonates including travertines from Tibet. In that context it is interesting to note, that the ^{234}U/^{238}U activity ratios of all sub-samples from all terraces are similar to each other (Table 3), indicating that the systematics have remained closed over that time period and that broadly similar hydrological regimes must have prevailed for these growth periods.

The travertine platform T1 is mainly composed of aragonite and likely precipitated from hydrothermal water similar or identical in its chemistry to the modern main hot spring. In a hydrothermal setting aragonite usually precipitates when spring temperatures are >40 °C and/or the Mg/Ca ratio is > 1.1 (Folk, 1994; Pentecost, 2005), but the presence of microbes can facilitate aragonite precipitation too (Guo and Riding, 1992; Folk, 1994). The modern main hot spring at Tirthapuri meets these conditions for aragonite precipitation (spring temperature ~72 °C, Mg/Ca ratio ~1.1; Tong et al., 2000) and microbial filaments are preserved in the aragonite layers from the travertine platform T1 (Fig. 8B). The well-developed lamination in these aragonite samples requires (i) carbonate
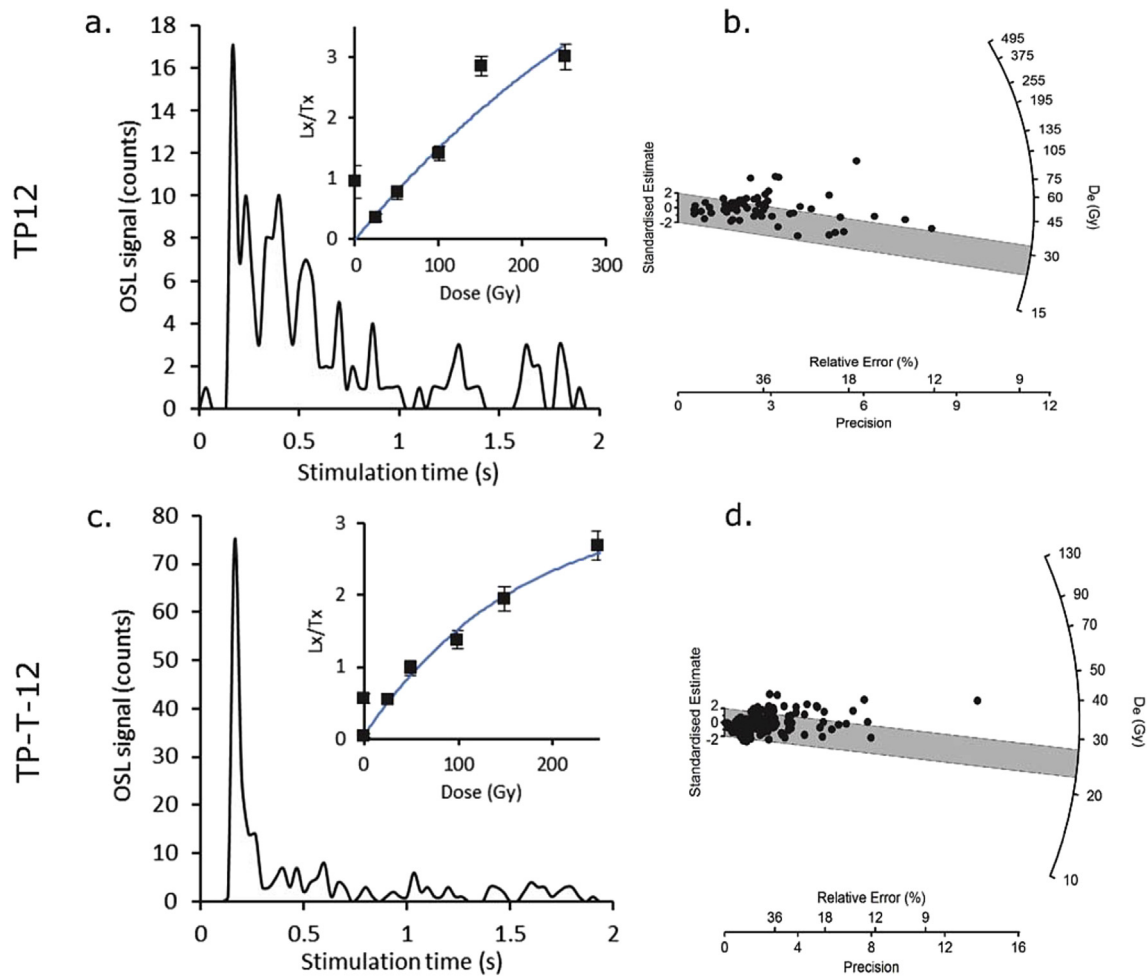
Fig. 9. OSL data from both sites investigated in this study. OSL decay curves (Tn) from a representative grains from sample TP-OSL-12 (A) and TP-T-12 (C) are shown. Insets to (A) and (C) show the corresponding dose-response curves. De distributions for TP-OSL-12 (B) and TP-T-12 (D) are shown on a radial plots, with the MAM De estimates shown as grey bars.

precipitation in flat terrain via sheet flow or in shallow pools (Chafetz and Folk, 1984; Guo and Riding, 1992), and (ii) a cyclic (likely seasonal) variation in the hydrochemistry of the spring water (e.g. changing water temperature and/or discharge rate in the course of a year; Guo and Riding, 1992; Folk, 1994). These petrographic observations fit nicely with the geomorphological setup of the platform; the main hot spring outlet is situated on top of this slightly convex travertine platform together with several active and fossil travertine pools (Fig. 6A). In concert these observations suggest that the main hot spring together with a few adjacent springs was probably responsible for precipitating the T1 travertine platform.

The hydrothermal carbonate that constitutes the travertine platform T2 as well as the associated travertine cones is characterized by cm-thick layers of dendrites alternating with mm-thick layers of clotted/peloidal micrite (Fig. 8C and D). Crystalline dendrites are a typical abiotic fabric in hydrothermal spring carbonates and usually form as a result of fast calcite precipitation that is driven by rapid CO_2 degassing from highly supersaturated (with respect to $CaCO_3$) spring water (Jones et al., 2005; Jones and Renaut, 2008; Rainey and Jones, 2009). A steady supply of hydrothermal water over smooth slopes or down inclined planes that allows rapid CO_2 degassing is required for growing such a dendritic fabric (Rainey and Jones, 2009; Gandin and Capezzuoli, 2014). Clotted

peloidal micrite in travertine is usually related to bacterial activity during summer, allowing microbial mats or biofilms to grow, providing a substrate for crystal nucleation (Rainey and Jones, 2009; Della Porta, 2015). The alternation of dendritic with clotted/peloidal micrite layers suggests a cyclic control on travertine growth (likely seasonal temperature variations and/or change in flow velocity; Jones and Renaut, 2008). The presence of numerous travertine cones on the T2 and T2$^{(1+)}$ platforms indicate the position of highly active paleo-spring orifices (Pentecost, 2005) and thus suggest that hot spring activity was more vigorous during the formation of the T2 platform compared to the formation of the T1 platform, which is characterized by flats and shallow pools (Pentecost, 2005).

The dense flowstone-like calcite that precipitated in a cavity inside a travertine cone from the T2 platform (Fig. 7C) is characterized by palisade columnar sparite (Fig. 8F), which usually precipitates from water with low calcite supersaturation under a low but constant discharge rate (Frisia et al., 2000). This cement indicates vadose conditions and might have formed from supersaturated meteoric percolation water and/or from hot spring water that re-infiltrated into the travertine cone. We favor the latter scenario, because although the travertine cone is ~4 m in size and the cavity is situated at the base of the cone, it is unlikely that this overburden was thick enough to allow percolation water of

meteoric origin to become supersaturated with respect to calcite. It is therefore suggested that re-infiltration of hydrothermal water was at least co-responsible for precipitating this flowstone.

Carbonate from the travertine platform T3 is made of mud-limestone (structureless micrite and microsparite; Fig. 8G) and such type of carbonate is often considered to be deposited in a stagnant aquatic environment, such as ponds or marshes, where the water is only slightly supersaturated with respect to calcite (Pedley, 1990; Sant'Anna et al., 2004; Croci et al., 2016). In such environments precipitation of micrite is often microbially mediated (Riding, 2000), but the input of hydrothermal water or evaporation can also lead to supersaturation and thus precipitation of mud-limestone (Pentecost, 2005; Capezzuoli et al., 2014). Indeed, the occurrence of layers composed of fan-like crystals alternating with micrite layers (Fig. 8H) points towards a mixed hydrothermal and meteoric origin of this fabric (Gandin and Capezzuoli, 2014), while detrital layers in some of the samples suggest repeated input of terrigenous material, possibly due to overland flow or via fluvial transport (Sant'Anna et al., 2004).

5.2. Understanding travertine deposition in relation to fluvial sedimentation

The investigated travertine platforms are sometimes deposited on bedrock but are mostly capping fluvial sediments (Figs. 6 and 7). We argue in the following that these platforms are adjusted to former floodplains of the Sutlej River and can be used to constrain the age of fluvial activity and also provide insights into the timing and process of fluvial down-cutting of the Menci basin and associated lowering of the groundwater table.

Outcrops in the travertine platforms T1 and T2 show that fluvial sediment is interbedded with travertine, preferentially at the platform base (in a semi-regular manner and successively thinning up-section; Figs. 6B and 7B), while evidence for a paleosol or a hiatus is missing (Fig. 7B). This suggests that fluvial sedimentation and precipitation of hydrothermal carbonate were operating next to each other and broadly simultaneously, at least at an initial stage of travertine platform formation. Travertine precipitation also caused cementation in the underlying gravel beds which show no evidence for weathering or soil formation (Fig. 6B). This also points towards a synchronicity of fluvial and incipient hydrothermal processes. Furthermore, the distal part of the travertine platform T1 is terraced and overlain by a thin veneer of fluvial gravels due to recurring inundation of this part of the travertine deposit by the Sutlej River during high discharge events (Fig. 4B). These sedimentological and geomorphological observations suggest that (i) (sub)recent travertine precipitation (platform T1) as well as past travertine precipitation (platform T2) both occurred on an active floodplain, (ii) the frequency of platform flooding and thus fluvial sediment input into the platform decreases while the travertine platform aggrades; consequently (iii) these travertine platforms T1 and T2 are interpreted to broadly mark the paleo-elevation of the Sutlej drainage system. This interpretation is sensible, given that spring emergence from a deep sub-surface and fault-bounded hydrothermal aquifer and associated travertine precipitation likely occur at the valley floor (cf. Özkul et al., 2014), similar to the modern situation at Tirthapuri, where hot springs emerge at or close to the modern river floodplain.

The carbonate platform on terrace T3 is also interpreted as a geomorphic and stratigraphic marker for a paleo-floodplain of the Sutlej River. This platform formed by hydrothermal water gathering in depressions such as marshes and ponds and via mixing with meteoric water causing mud limestone to precipitate. Occasional sand layers suggest input of detrital material likely via fluvial processes. This mud limestone partly overlies coarse fluvial gravels and

both sediments show a similarly high degree of weathering (Fig. 7D). The terrace generation T3 is characterized by particularly wide terrace treads (Figs. 2 and 5A) and for the carbonate platform T3 we thus envisage travertine precipitation in a broad paleo-valley slightly distal to the paleo-floodplain of the Sutlej River.

5.3. Timing of travertine deposition, fluvial terrace formation and alluvial fan activity

Most travertines are characterized by precipitation rates ≥ 1 cm/yr due to the typically high degree of supersaturation of hydrothermal water with respect to calcite from which they precipitate (Pentecost, 2005; Capezzuoli et al., 2014; Wang et al., 2016; Meyer et al., 2017). The travertine samples from the T1 and T2 travertine platforms at Tirthapuri are laminated on the cm-scale (average thickness of ~0.4–1.5 cm for the platforms T1 and T2, respectively) which, under the (reasonable) assumption that this lamination is indeed annual in nature, suggests that these platforms aggraded in the course of several centuries to a few millennia at most. Sedimentological evidence further indicates that, at the initial stage of travertine platform formation, precipitation of hydrothermal carbonate probably occurred in or at close vertical distance to an active floodplain. We therefore interpret the ^{230}Th/U ages of the samples TP-T-1 (travertine platform T3: 127.5 ± 1.1 ka) and TP-T-15 (travertine cone on top of travertine platform T2: 10.0 ± 0.2 ka) as minimum age constraints of the underlying fluvial sediments (i.e. the fluvial gravels should have the same or a slightly higher age compared to the capping travertine; Fig. 10). This interpretation is in general agreement with the OSL age of 13.6 ± 1.7 ka (sample TP-T-12) from the travertine-cemented fluvial sands that directly underlie the travertine platform T2.

The ^{230}Th/U ages of the flowstone sample TP-T-16 taken from a small cavity inside the same travertine cone that has been dated to 10.0 ± 0.2 ka (sample TP-T-15; Fig. 7C) suggest that vadose calcite precipitation inside this cone lasted from ca. 9.7 to 8.8 ka (Table 3). Geochemical considerations suggest that re-infiltration of hydrothermal water is required for precipitating a calcitic flowstone inside this travertine cone. For the travertine platform T2, these ^{230}Th/U ages in conjunction with sedimentological and geochemical considerations indicate that hydrothermal activity started in the early Holocene and lasted until 8.8 ± 0.8 ka. Furthermore, fluvial incision must have started at a very early stage of platform formation, ultimately avoiding erosion of these travertine deposits by the Sutlej River, as evidenced by the fact that (i) numerous travertine cones are preserved on top of T2 despite the highly confined setting (the Sutlej River has started cutting a bedrock gorge immediately south of the T2 and T3 platforms; Figs. 2 and 3B) and that (ii) fluvial sediment is lacking in the upper sections of these platforms.

The weighted mean ^{230}Th/U age of 0.22 ± 0.03 ka for the travertine samples TP-T-6a to 6c suggests an almost modern age for the top part of the T1 travertine platform from which samples were collected. These ages and the observation that this relatively soft aragonitic deposit is preserved next to the modern Sutlej River suggest that fluvial incision has arrived at the modern level at least 0.2 ka ago and that lateral erosion since that time has been limited (Fig. 10). The exact relation of this travertine platform with the fluvial terraces is more difficult to decipher. The distal part of the T1 platform is terraced and correlates in altitude with the fluvial terrace T1$^{(1-)}$ but absolute age constrains for this or other T1 sub-terraces are missing.

No absolute age control for the terrace T4 (at ~4600 m asl.) or the paleosurface that occurs at ~4650 m asl. are available. However, the Early Pleistocene age of the Xiangzi formation that underlies this paleosurface (Fig. 2; Meng et al., 2008) indicates that (i) the
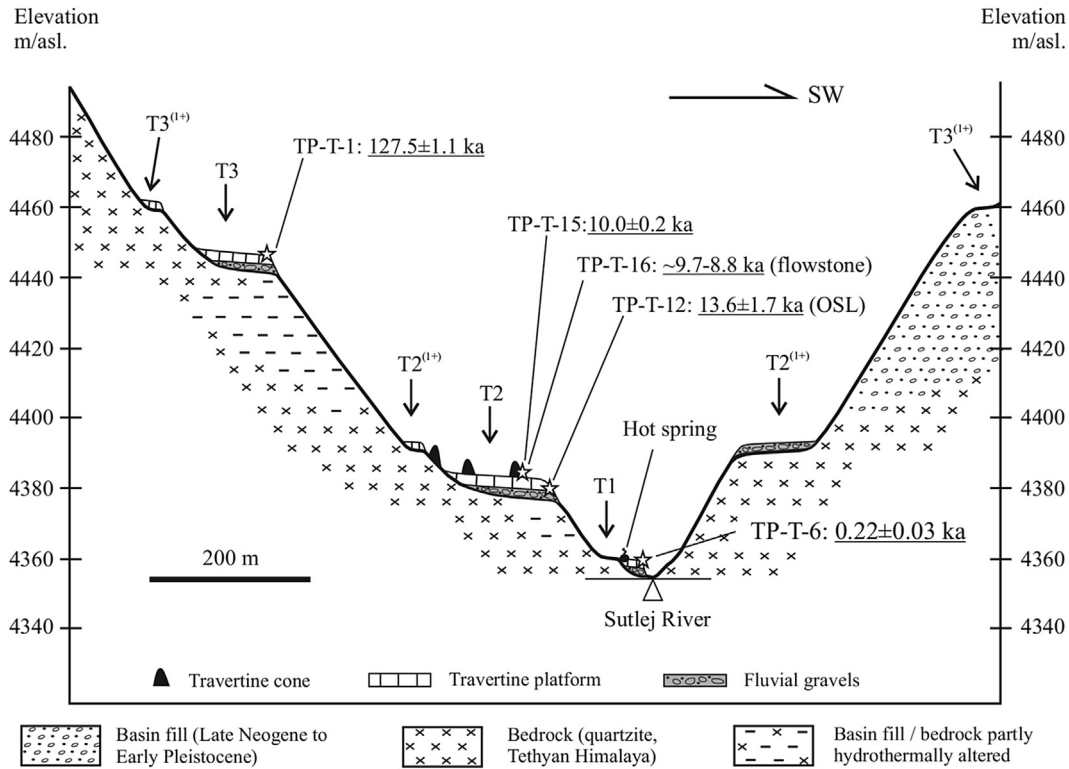
Fig. 10. Schematic valley cross-profile of the Sutlej River next to the Tirthapuri hot springs (profile section B-B′, compare Fig. 3B) showing compiled stratigraphic and chronologic information.

highest level of basin infill was achieved ca. ≥0.78 Ma ago and (ii) the shift from an aggradational to an erosive fluvial regime in the upper Sutlej drainage occurred around that time.

In the Menci basin modern and sub-recent alluvial activity is restricted to a few sparsely vegetated fans that are fed by ephemeral gullies or streams (Fig. 2). Noticeable are big alluvial fans that are adjusted to the T2 terraces and often laterally merge into each other (Figs. 2 and 4B, C). The weighted mean OSL age of 9.1 ± 0.7 ka for the alluvial fan that accumulated on the T2$^{(1+)}$ (Figs. 3C and 4C) in combination with the sedimentology of this fan imply a rapid response of the hill slope to an increased availability of water/runoff causing liquefied mass flows to accumulate. The optical age of this fan is concordant with the ^{230}Th/U age of the T2 travertine platform and also corroborates our terrace stratigraphy; the fan overlies the T2$^{(1+)}$ terrace which is ~15 m higher than T2 (Fig. 3D), and, thus, must be older than ca. 9 ka. Given that fans graded to the T2$^{(1+)}$ terrace make up a significant proportion of all the alluvial fans that can be mapped in the central Menci basin (~50% aerial extent), it is concluded that sediment supply from hillslopes was strongly enhanced during the time of T2 terrace formation, likely leading to a pulse of alluvial fan activity.

5.4. Climatic versus tectonic controls on fluvial terrace formation

Fluvial terrace formation is influenced by a variety of intrinsic and extrinsic factors. On the scale of very large catchments such as the Sutlej (5th order stream and ~5.3 × 10^4 km^2 at Tirthapuri) and orogenic timescales, coupling of erosional processes with tectonics and/or climate are fundamental for alluvial aggradation and incision (Wegmann and Pazzaglia, 2002, 2009; Starkel, 2003; Bridgland and Westaway, 2008; Garcia and Mahan, 2014).

The Menci basin as well as the Tirthapuri hot springs are bound to the Karakorum fault system (Fig. 1), which is characterized by right lateral strike-slip, pull-apart kinematics and slip rates in the order of ~6–10 mm/yr (Murphy et al., 2000; Wang et al., 2008a; Chevalier et al., 2005). These faults are likely influencing the course of the Sutlej River by determining zones of weak bedrock and thus preferential fluvial incision, and it is suspected that the hot springs as well as the adjacent bedrock gorge are controlled by such a shear zone (Fig. 3). In our investigation area and over the investigated time range (last ca. 130 ka), we do not expect that strike-slip movement along these faults or pull-apart kinematics have significantly impacted on the vertical terrace positions and, thus terrace stratigraphy. Accordingly, no geomorphological or sedimentological indication for such vertical displacements has been observed.

Knickpoint migration due to surface or rock uplift and/or base level fall are important tectonic factors controlling channel incision and terrace formation (Wegmann and Pazzaglia, 2002, 2009; Starkel, 2003). Towards the north and northwest, the Menci basin is situated ~50 km from the drainage divide with a constant gradient of ~6 m/km for the entire east-west trending reach of the Sutlej (~273 km) before it is turning south and cutting through the High Himalaya. A knickpoint can be identified downstream of the Menci basin, near the Indian-China border, where the Sutlej River crosses the Leo Pargil Range. Late Pleistocene alluvial aggradation and incision in the Menci basin are thus regarded as being largely unaffected by tectonic factors, and similar conclusions have been drawn from investigating Pleistocene valley fills in the headwaters of the Zanskar and Indus rivers, respectively (Munack et al., 2016). We rather anticipate that in the cold-arid setting of southwestern Tibet climate and in particular variation in the strength of the ISM played a fundamental role in terrace formation.

Numerous speleothem oxygen-isotope (δ^{18}O) records from Asia (including records from the Tibetan Plateau, the Himalaya and the Indian Subcontinent; Figs. 1A and 11) reveal that (i) the ISM
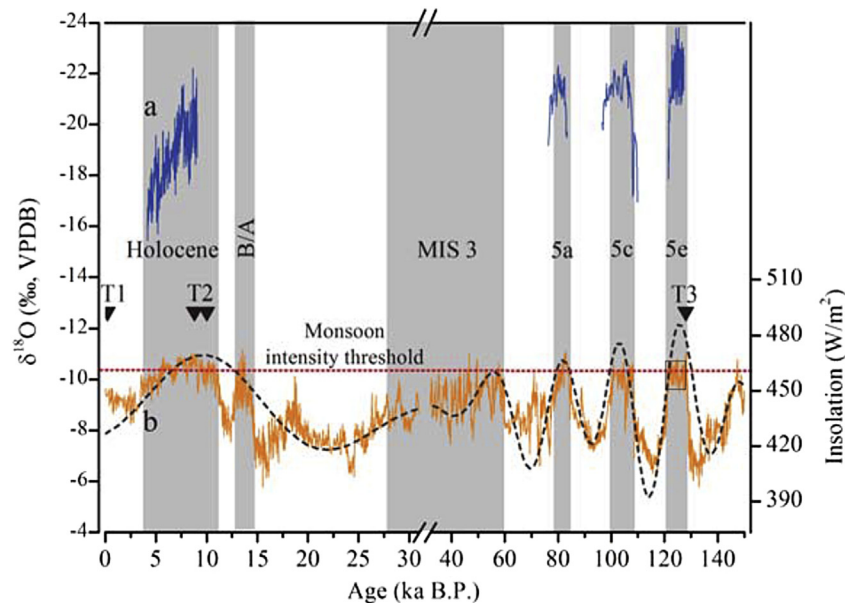
Fig. 11. Comparison of travertine precipitation periods at Tirthapuri (black triangles represent travertine ^{230}Th/U ages discussed in text) with cave speleothem δ^{18}O records showing the Asian summer monsoon variability during the past 150 ka. T1 to T3: travertine platform T1 to T3. Note that the scale on the x-axis is different before and after 32 ka. a — Tianmen cave (central Tibet; Cai et al., 2010, 2012); b — East Asia summer monsoon record (compilation of 3 speleothem records from southern China; Cheng et al., 2016); Black dashed line is the 21st July insolation at 65°N (Berger and Loutre, 1991). Periods of more negative speleothem δ^{18}O values indicate times of enhanced monsoon intensity and are highlighted by grey bars (based on Cheng et al., 2016). B/A is the Bölling/Alleröd interstadial. The red dashed line in b indicates a semi-quantitative threshold in monsoon intensity upon which travertine precipitation in the cold-arid catchment of the upper Sutlej probably commences (based on the average δ^{18}O isotope values in the East Asia summer monsoon record during the time periods of T2 and T3 travertine platform formation (i.e. −10.4‰)). (For interpretation of the references to colour in this figure legend, the reader is referred to the web version of this article.)

fluctuated over millennial to orbital time-scales in response to changes in Northern Hemisphere summer insolation and (ii) these oscillations were broadly synchronous, suggesting that continent-scale monsoonal circulation changes were a simultaneous phenomenon (Fig. 11; Fleitmann et al., 2003; Sinha et al., 2005; Cai et al., 2010, 2012; Dutt et al., 2015; Cheng et al., 2016; Kathayat et al., 2016). These variations in the intensity of the ISM are also mirrored in lacustrine archives of several Tibetan lakes (Sumxi Co, Van Campo and Gasse, 1993; Tso Kar, Demske et al., 2009; Nam Co, Zhu et al., 2015; Baqan Co, Huth et al., 2015; Nganglan Ring Co, Hudson et al., 2015; Paiku Co, Wünnemann et al., 2015; compare Fig. 1A for locations). Furthermore, current research and improved surface-exposure and luminescence dating chronologies suggest that in southern Tibet and the Himalaya ISM oscillations exerted a profound control on landscape evolution via erosional hillslope processes, river discharge, and sedimentation flux (Pratt et al., 2002; Brown et al., 2003; Pratt-Sitaula et al., 2004; Bookhagen et al., 2005, 2006; Srivastava et al., 2008, 2009; Juyal et al., 2010; Thakur et al., 2014; Densmore et al., 2016; Dey et al., 2016). This concept of climate forcing of sediment cycles is particularly well investigated along the middle and lower reaches of the Sutlej River and adjacent catchments, which are characterized by high monsoon precipitation and relatively mild temperatures (MAP of 760—1320 mm/yr; MAT of 14—28 °C; Singh et al., 2015). The emerging view for these strongly monsoon influenced settings is that strengthening of the ISM between ~15 and 10 ka caused rapid sediment aggradation (Bookhagen et al., 2006; Thakur et al., 2014; Densmore et al., 2016) quickly followed by incision at a time when the ISM was still very strong (i.e. at ~9.3 ka in the case of the lower Sutlej River; Dey et al., 2016). Repeated regional incision phases occurred from ~8 ka onward in line with the overall decreasing ISM intensity (Bookhagen et al., 2006; Dey et al., 2016; Cheng et al., 2016). For the lower Sutlej River it is suspected that the onset of incision at ~9.3 ka was linked to an overall decrease in the sediment

flux from the hillslopes, because the easily eroded sediments had been removed from the source areas during the initial ISM strengthening phase (~15—10 ka) (Dey et al., 2016). This phenomenon of pulses of hill-slope driven aggradation during periods of increasing precipitation followed by incision during the waning stages of peak precipitation has been observed in other mountain ranges as well, including NW Argentina (Schildgen et al., 2016), the Pamir (Strecker et al., 2003) the Tien Shan (Huang et al., 2014) or the Appeninies (Wegmann and Pazzaglia, 2009).

The climatic and geomorphologic setting in the upper Sutlej is significantly different compared to that in its middle and lower reaches, with MAP of only ~250 mm/yr, MAT of 0—3 °C and relatively wide basins between 4300 and 4600 m asl. that are fed by rivers originating in the Transhimalaya (~25 km to the north) or the High Himalaya (~80 km to the south). Despite this cold and arid setting, the ISM is still the main source of precipitation delivering >70% of the MAP to the upper Sutlej (Bookhagen and Burbank, 2010). Our ^{230}Th/U and OSL ages from the travertine platform T2 suggest that hot spring activity and hydrothermal carbonate precipitation started 10.0 ± 0.2 ka ago and lasted until 8.8 ± 0.8 ka, and thus precisely coincide with the time when the ISM strength was at its maximum (Cai et al., 2012; Cheng et al., 2016, Fig. 11). Isotopic groundwater studies from Tibet show that (i) hydrothermal spring water is mainly recharged via atmospheric precipitation and that (ii) groundwater circulation on the plateau is rapid and thus residence times for hydrothermal water are short (i.e. a few decades; Tan et al., 2014). We thus suggest that hot spring activity at Tirthapuri is directly related to strong phases of the ISM and such links have already been put forward for the Nyalam travertine (Zentmyer et al., 2008) and the Chusang travertine (Wang et al., 2016; Meyer et al., 2017; both southern Tibet; Fig. 1).

OSL dating in conjunction with geomorphologic and sedimentological data from the T2 travertine platform and terraces further suggest that (i) a short pulse of valley aggradation prior to

travertine formation occurred and lasted until 13.6 ± 1.7 ka; (ii) fluvial incision commenced at a very early stage of travertine platform formation – essentially during peak monsoon conditions; and (iii) local hill-slopes responded rapidly to an enhanced ISM via alluvial fan activity at 9.1 ± 0.7 ka. These observations strongly support the hypothesis of climate forcing of sediment cycles as outlined above. We speculate that the material flushed from hill-slopes during the early Holocene peak in monsoon activity was mainly transferred and stored within alluvial fans along the valley margins, and did thus not result in significant valley floor aggradation in the wide pull-apart setting of the central Menci basin. This interpretation is supported by our geomorphological maps (Figs. 2 and 4), which indicate that although a significant proportion of alluvial fans are adjusted to the $T2^{(1+)}$ and T2 terraces, they are all concentrated along the valley flanks and rarely reached the contemporaneous active river channel.

The ^{230}Th/U age of 127.5 ± 1.1 ka for the travertine platform T3 (Fig. 10) suggests that the valley floor in the central Menci basin was ~93 m higher during the last interglacial and ~28 m higher during the early Holocene compared to today. We point out that the precision on this ^{230}Th/U age (0.87% relative error) is good enough to suggest that this age probably coincides with the insolation maximum (at ca. 128 ka; Berger and Loutre, 1991) and thus the beginning of the last interglacial (MIS 5e, lasting from ca. 130–120 ka; Cai et al., 2010; Kathayat et al., 2016; Cheng et al., 2016, Fig. 11). Furthermore, we observe that, like travertine platform T2, a few meters of T3 fluvial gravels are overlying bedrock and are capped by hydrothermal carbonate. The same sequence of events that operated during the early Holocene is thus envisaged for the formation of the travertine platform T3 at the beginning of MIS 5e: the insolation-driven intensification of the ISM caused a short pulse of fluvial aggradation and activated hydrothermal springs and travertine precipitation which, in turn, is immediately followed by fluvial incision and thus terrace formation.

Based on our combined ^{230}Th/U ages and terrace stratigraphy, average incision rates for the upper Sutlej at Tirthapuri can be obtained. First a semi-quantitative threshold in monsoon intensity is defined, upon which travertine precipitation in the catchment of the upper Sutlej probably commences. This threshold is based on the average δ^{18}O isotope values in the East Asia summer monsoon record during the time periods of T2 and T3 travertine platform formation (−10.4‰; red dashed line in Fig. 11). Time periods with δ^{18}O isotope values more negative than −10.4‰ are considered wet enough to allow for significant travertine precipitation followed by fluvial down cutting and thus terrace formation as outlined above (i.e. MIS 5e, 5c, 5a, the Bölling Alleröd and from ca. 11.7–5 ka; Fig. 11). Considering only periods above the monsoon intensity threshold we obtain average incision rates of ~4.2 mm/yr for the Holocene or ~2–3 mm/yr for the past ~128 ka. These incision rates are at the lower end compared to the incision rates obtained for the High Himalaya (~2–12 mm/yr; Burbank et al., 1996; Vance et al., 2003; Pratt-Sitaula et al., 2004) but such comparisons have to be treated with caution. Firstly, because at Tirthapuri the Sutlej re-incises into sedimentary basin fill rather than bedrock, and secondly because of the overall lower discharge and valley steepness in the upper Sutlej setting relative to the High Himalaya. A complicating factor at Tirthapuri is the complex nature of longer-term erosion characterized by varying relative contributions of rapid vertical incision with valley-bottom narrowing, and phases of slower lateral erosion and valley-bottom widening (Hancock and Anderson, 2002; Wegmann and Pazzaglia, 2002, 2009; DeVecchio et al., 2012; Garcia and Mahan, 2014; Malatesta et al., 2016). Following these millennial-scale pulses of dominantly discharge-driven vertical incision during peak monsoon times, fluvial dynamics would return to a transport-limited system with prolonged phases of lateral erosion and valley widening. This would lead to the removal of previously formed strath or fill-cut terraces (Wegmann and Pazzaglia, 2002; Limaye and Lamb, 2016), limits the longer-term preservation of more complete terrace sequences, e.g. as represented by the multiple Holocene terrace sub-levels at Tirthapuri (Fig. 3A, C), and confirms that the interpretation of long-term fluvial incision rates may not be straightforward (Finnegan et al., 2014). Phases of vertical incision therefore represent dynamic but episodic landscape-scale events in our combined model of ISM driven travertine and terrace formation in the upper Sutlej (Fig. 11).

6. Conclusions

Hot spring activity and thus extensive hydrothermal carbonate precipitation and formation of travertine platforms at Tirthapuri (upper Sutlej) are linked to phases of maximum strength of the ISM. These travertine platforms started to aggrade in or adjacent to active fluvial channels and were preserved from fluvial erosion because the enhanced ISM also triggered river bed incision and lowering of the local groundwater table eventually cutting off the travertine mounds and cones from hot water supply. Therefore these fossil travertine platforms indicate the altitude of former river beds and the timing when fluvial down-cutting commenced, and are thus regarded valuable geomorphological markers for the reconstruction of late Quaternary landscape and climate dynamics, and chronological markers suitable for the application of U-Th dating techniques. This is particularly evident in high-mountain settings such as the Tibetan Plateau where (i) travertine formation is facilitated by active tectonics, (ii) long-term preservation potential for alluvial sediment may be limited, and (iii) the establishment of terrace chronologies is additionally complicated due to the coarse character of alluvial sediment. In such a setting, the upper Sutlej is characterized by (i) a series of high altitude pull-apart basins and (ii) arid conditions due to its position downward of the Himalaya and the Karakoram that are partly blocking the ISM and the westerlies, respectively. We argue that because of this arid setting and the relative importance of the ISM for the MAP in the upper Sutlej (175 mm or 70% of the MAP are currently delivered via the ISM), the travertine deposits at Tirthapuri can also be interpreted as sensitive indicators of peak ISM conditions. ^{230}Th/U dating in combination with OSL dating constrains two such intervals when the ISM was able to penetrate into southwestern Tibet triggering an instantaneous and significant landscape response: during the early Holocene (ca. 10.0–8.8 ka) and at the beginning of the MIS 5e (ca. 128 ka). At these times the ISM was strong enough in this arid landscape and activated hot springs and travertine precipitation, facilitated fluvial incision and stripped off sediments from the regional hill-slopes at rates significantly higher compared to times with lower insolation and thus a regionally stagnant monsoon.

References

Aitchison, J.C., Davis, A.M., Badengzhu, B., Luo, H., 2002. New constraints on the India-Asia collision: the lower Miocene gangrinboche conglomerates, Yarlung Tsangpo suture zone, SE Tibet. J. Asian Earth Sci. 21 (3), 251–263.

Armijo, R., Tapponnier, P., Mercier, J.L., Han, T.L., 1986. Quaternary extension in southern Tibet - field observations and tectonic implications. J. Geophys. Res. 91 (B14), 13803–13872.

Armijo, R., Tapponnier, P., Tonglin, H., 1989. Late cenozoic right-lateral strike-slip faulting in southern Tibet. J. Geophys. Res. 94 (B3), 2787–2838.

Berger, A., Loutre, M.F., 1991. Insolation values for the climate of the last 10000000 years. Quat. Sci. Rev. 10 (4), 297–317.

Blisniuk, P.M., Hacker, B.R., Glodny, J., Ratschbacher, L., Bi, S.W., Wu, Z.H., McWilliams, M.O., Calvert, A., 2001. Normal faulting in central Tibet since at least 13.5 Myr ago. Nature 412 (6847), 628–632.

Bookhagen, B., Burbank, D.W., 2010. Toward a complete Himalayan hydrological budget: spatiotemporal distribution of snowmelt and rainfall and their impact on river discharge. J. Geophys. Res. 115, F03019.

Bookhagen, B., Fleitmann, D., Nishiizurrli, K., Strecker, M.R., Thiede, R.C., 2006. Holocene monsoonal dynamics and fluvial terrace formation in the northwest Himalaya, India. Geology 34 (7), 601–604.

Bookhagen, B., Thiede, R.C., Strecker, M.R., 2005. Late Quaternary intensified monsoon phases control landscape evolution in the northwest Himalaya. Geology 33 (2), 149–152.

Bøtter-Jensen, L., Andersen, C.E., Duller, G.A.T., Murray, A.S., 2003. Developments in radiation, stimulation and observation facilities in luminescence measurements. Radiat. Meas. 37 (4–5), 535–541.

Bøtter-Jensen, L., Mejdahl, V., 1988. Assessment of beta dose-rate using a GM multicounter system. Nucl. Tracks Radiat. Meas. 14, 187–191.

Bridgland, D., Westaway, R., 2008. Climatically controlled river terrace staircases: a worldwide Quaternary phenomenon. Geomorphology 98 (3–4), 285–315.

Brown, E.T., Bendick, R., Bourles, D.L., Gaur, V., Molnar, P., Raisbeck, G.M., Yiou, F., 2003. Early Holocene climate recorded in geomorphological features in Western Tibet. Palaeogeogr. Palaeoclimatol. Palaeoecol. 199 (1–2), 141–151.

Burbank, D.W., Leland, J., Fielding, E., Anderson, R.S., Brozovic, N., Reid, M.R., Duncan, C., 1996. Bedrock incision, rock uplift and threshold hillslopes in the northwestern Himalayas. Nature 379 (6565), 505–510.

Cai, Y., Cheng, H., An, Z., Edwards, R.L., Wang, X., Tan, L., Wang, J., 2010. Large variations of oxygen isotopes in precipitation over south-central Tibet during Marine Isotope Stage 5. Geology 38 (3), 243–246.

Cai, Y., Fung, I., Edwards, R.L., An, Z., Cheng, H., Lee, J.E., Tan, L., Sheng, C.C., Wang, X., Day, J.A., Zhou, W., Kelly, M.J., Chiang, J.C.H., 2015. Variability of stalagmite-inferred Indian monsoon precipitation over the past 252,000 y. Proc. Natl. Acad. Sci. U. S. A. 112 (10), 2954–2959.

Cai, Y., Zhang, H., Cheng, H., An, Z., Edwards, R.L., Wang, X., Tan, L., Liang, F., Wang, J., Kelly, M., 2012. The Holocene Indian monsoon variability over the southern Tibetan Plateau and its teleconnections. Earth Planet. Sci. Lett. 335, 135–144.

Capezzuoli, E., Gandin, A., Pedley, M., 2014. Decoding tufa and travertine (fresh water carbonates) in the sedimentary record: the state of the art. Sedimentology 61 (1), 1–21.

Chafetz, H.S., Folk, R.L., 1984. Travertines — depositional morphology and the bacterially constructed constituents. J. Sediment. Pet. 54 (1), 289–316.

Cheng, H., Edwards, R.L., Hoff, J., Gallup, C.D., Richards, D.A., Asmerom, Y., 2000. The half-lives of uranium-234 and thorium-230. Chem. Geol. 169 (1–2), 17–33.

Cheng, H., Edwards, R.L., Sinha, A., Spotl, C., Yi, L., Chen, S.T., Kelly, M., Kathayat, G., Wang, X.F., Li, X.L., Kong, X.G., Wang, Y.J., Ning, Y.F., Zhang, H.W., 2016. The Asian monsoon over the past 640,000 years and ice age terminations. Nature 534 (7609), 640–646.

Chevalier, M.L., Ryerson, F.J., Tapponnier, P., Finkel, R.C., Van der Woerd, J., Li, H.B., Liu, Q., 2005. Slip-rate measurements on the Karakorum Fault may imply secular variations in fault motion. Science 307 (5708), 411–414.

CIGMR (Chengdu Institute of Geology and Mineral Resources), G.S.o.C, 2004. Geological Map of Qinghai-tibet Plateau and Adjacent Region (Scale: 1:1 500 000). Chengdu. Cartographic Publishing House, Chengdu.

Croci, A., Della Porta, G., Capezzuoli, E., 2016. Depositional architecture of a mixed travertine-terrigenous system in a fault-controlled continental extensional basin (Messinian, Southern Tuscany, Central Italy). Sediment. Geol. 332, 13–39.

DeCelles, P.G., Kapp, P., Quade, J., Gehrels, G.E., 2011. Oligocene-Miocene Kailas basin, southwestern Tibet: record of postcollisional upper-plate extension in the Indus-Yarlung suture zone. Geol. Soc. Am. Bull. 123 (7–8), 1337–1362.

Della Porta, G., 2015. Special Publications. Carbonate Build-ups in Lacustrine, Hydrothermal and Fluvial Settings: Comparing Depositional Geometry, Fabric Types and Geochemical Signature, vol. 418. Geological Society, London, pp. 17–68 (1).

Demske, D., Tarasov, P.E., Wünnemann, B., Riedel, F., 2009. Late glacial and Holocene vegetation, Indian monsoon and westerly circulation in the Trans-Himalaya recorded in the lacustrine pollen sequence from Tso Kar, Ladakh, NW India. Palaeogeogr. Palaeoclimatol. Palaeoecol. 279 (3–4), 172–185.

Densmore, A.L., Sinha, R., Sinha, S., Tandon, S.K., Jain, V., 2016. Sediment storage and release from Himalayan piggyback basins and implications for downstream river morphology and evolution. Basin Res. 28 (4), 446–461.

DeVecchio, D.E., Heermance, R.V., Fuchs, M., Owen, L.A., 2012. Climate-controlled landscape evolution in the western transverse ranges, California: insights from quaternary geochronology of the saugus formation and strath terrace flights.

Lithosphere 4 (2), 110–130.

Dey, S., Thiede, R.C., Schildgen, T.F., Wittmann, H., Bookhagen, B., Scherler, D., Jain, V., Strecker, M.R., 2016. Climate-driven sediment aggradation and incision since the late Pleistocene in the NW Himalaya, India. Earth Planet. Sc. Lett. 449, 321–331.

Duller, G.A.T., 2003. Distinguishing quartz and feldspar in single grain luminescence measurements. Radiat. Meas. 37 (2), 161–165.

Dutt, S., Gupta, A.K., Clemens, S.C., Cheng, H., Singh, R.K., Kathayat, G., Edwards, R.L., 2015. Abrupt changes in Indian summer monsoon strength during 33,800 to 5500years BP. Geophys. Res. Lett. 42 (13), 5526–5532.

Finnegan, N.J., Hallet, B., Montgomery, D.R., Zeitler, P.K., Stone, J.O., Anders, A.M., Yuping, L., 2008. Coupling of rock uplift and river incision in the Namche Barwa-Gyala Peri massif. Tibet. Geol. Soc. Am. Bull. 120 (1–2), 142–155.

Finnegan, N.J., Rina Schumer, R., Finnegan, S., 2014. A signature of transience in bedrock river incision rates over timescales of 104-107 years. Nature 505 (7483), 391–394.

Fleitmann, D., Burns, S.J., Mudelsee, M., Neff, U., Kramers, J., Mangini, A., Matter, A., 2003. Holocene forcing of the Indian monsoon recorded in a stalagmite from Southern Oman. Science 300 (5626), 1737–1739.

Folk, R.L., 1994. Interaction between bacteria, nannobacteria, and mineral precipitation in hot-springs of Central Italy. Géogr. Phys. Quat. 48 (3), 233–246.

Frisia, S., Borsato, A., Fairchild, I.J., McDermott, F., 2000. Calcite fabrics, growth mechanisms, and environments of formation in speleothems from the Italian alps and southwestern Ireland. J. Sediment. Res. 70 (5), 1183–1196.

Galbraith, R.F., Roberts, R.G., Laslett, G.M., Yoshida, H., Olley, J.M., 1999. Optical dating of single and multiple grains of quartz from Jinmium rock shelter, northern Australia: part I, experimental design and statistical models. Archaeometry 41, 339–364.

Galbraith, R., 2003. A simple homogeneity test for estimates of dose obtained using OSL. Anc. TL 21, 75–77.

Gandin, A., Capezzuoli, E., 2014. Travertine: distinctive depositional fabrics of carbonates from thermal spring systems. Sedimentology 61 (1), 264–290.

Garcia, A.F., Mahan, S.A., 2014. The notion of climate-driven strath-terrace production assessed via dissimilar stream-process response to late Quaternary climate. Geomorphology 214, 223–244.

Gliganic, L.A., May, J.-H., Cohen, T.J., 2015. All mixed up: using single-grain equivalent dose distributions to identify phases of pedogenic mixing on a dryland alluvial fan. Quat. Int. 362, 23–33.

Guérin, G., Mercier, N., Adamiec, G., 2011. Dose-rate conversion factors: update. Anc. TL 29, 5–8.

Guo, L., Riding, R., 1992. Aragonite laminae in hot water travertine crusts, Rapolano-Terme, Italy. Sedimentology 39 (6), 1067–1079.

Hancock, G.S., Anderson, R.S., 2002. Numerical modeling of fluvial strath-terrace formation in response to oscillating climate. Geol. Soc. Am. Bull. 114 (9), 1131–1142.

Hodges, K.V., 2000. Tectonics of the Himalaya and southern Tibet from two perspectives. Geol. Soc. Am. Bull. 112 (3), 324–350.

Hoffmann, D.L., Prytulak, J., Richards, D.A., Elliott, T., Coath, C.D., Smart, P.L., Scholz, D., 2007. Procedures for accurate U and Th isotope measurements by high precision MC-ICPMS. Int. J. Mass Spectrom. 264 (2–3), 97–109.

Hoffmann, D.L., 2008. 230Th isotope measurements of femtogram quantities for U-series dating using multi ion counting (MIC) MC-ICPMS. Int. J. Mass Spectrom. 275 (1–3), 75–79.

Hoffmann, D.L., Pike, A.W.G., García-Diez, M., Pettitt, P.B., Zilhão, J., 2016. Methods for U-series dating of CaCO3 crusts associated with Palaeolithic cave art and application to Iberian sites. Quat. Geochronol. 36, 104–119.

Huang, W.-l., Yang, X.-p., Li, A., Thompson, J.A., Zhang, L., 2014. Climatically controlled formation of river terraces in a tectonically active region along the southern piedmont of the Tian Shan, NW China. Geomorphology 220, 15–29.

Hudson, A.M., Quade, J., Huth, T.E., Lei, G., Cheng, H., Edwards, L.R., Olsen, J.W., Zhang, H., 2015. Lake level reconstruction for 12.8–2.3 ka of the Ngangla Ring Tso closed-basin lake system, southwest Tibetan Plateau. Quat. Res. 83 (1), 66–79.

Huntley, D.J., Godfrey-Smith, D.I., Thewalt, M.L.W., 1985. Optical dating of sediments. Nature 313, 105–107.

Huth, T., Hudson, A.M., Quade, J., Guoliang, L., Hucai, Z., 2015. Constraints on paleoclimate from 11.5 to 5.0 ka from shoreline dating and hydrologic budget modeling of Baqan Tso, southwestern Tibetan Plateau. Quat. Res. 83 (1), 80–93.

Jones, B., Renaut, R.W., 2008. Cyclic development of large, complex, calcite dendrite crystals in the Clinton travertine, Interior British Columbia, Canada. Sediment. Geol. 203 (1–2), 17–35.

Jones, B., Renaut, R.W., Owen, R.B., Torfason, H., 2005. Growth patterns and implications of complex dendrites in calcite travertines from Lysuholl, Sn ae fellsnes. Icel. Sedimentol. 52 (6), 1277–1301.

Juyal, N., Sundriyal, Y., Rana, N., Chaudhary, S., Singhvi, A.K., 2010. Late quaternary fluvial aggradation and incision in the monsoon-dominated alaknanda valley, central Himalaya, Uttrakhand, India. J. Quat. Sci. 25 (8), 1293–1304.

Kaiser, K., Lai, Z.P., Schneider, B., Junge, F.W., 2010. Late Pleistocene genesis of the middle Yarlung Zhangbo Valley, southern Tibet (China), as deduced by sedimentological and luminescence data. Quat. Geochronol. 5 (2–3), 200–204.

Kathayat, G., Cheng, H., Sinha, A., Spotl, C., Edwards, R.L., Zhang, H.W., Li, X.L., Yi, L., Ning, Y.F., Cai, Y.J., Lui, W.G.L., Breitenbach, S.F.M., 2016. Indian monsoon variability on millennial-orbital timescales. Sci. Rep. 6, 24374,. http://dx.doi.org/10.1038/srep24374.

Kempf, O., Blisniuk, P.M., Wang, S.F., Fang, X.M., Wrozyna, C., Schwalb, A., 2009.

Sedimentology, sedimentary petrology, and paleoecology of the monsoon-driven, fluvio-lacustrine Zhada Basin, SW-Tibet. Sediment. Geol. 222 (1–2), 27–41.

Kirby, E., Whipple, K.X., Tang, W., Chen, Z., 2003. Distribution of active rock uplift along the eastern margin of the Tibetan Plateau: inferences from bedrock channel longitudinal profiles. J. Geophys. Res. 108, 2217. http://dx.doi.org/10.1029/2001JB000861.

Li, Q., Wang, S.Q., Xie, G.P., 2011. Discovery of fossil equss near menshi (moincer, or Menci), ngari, Xizang (Tibet). Quat. Sci. 31 (4), 689–698 (in Chinese with English abstract).

Li, B.Y., Wang, F.B., Zhang, Q.S., 1983. The Series of the Scientific Expedition to the Qinghai-tibet Plateau, Quaternary Geology of Tibet. Science Press, Beijing (in Chinese).

Li, Y.Z., 2006. Xizang Annual. Tibet People Publishing Hause, Lhasa (in Chinese).

Limaye, A.B.S., Lamb, M.P., 2016. Numerical model predictions of autogenic fluvial terraces and comparison to climate change expectations. J. Geophys. Res. 121, 512–544.

Love, K.M., Chafetz, H.S., 1988. Diagenesis of laminated travertine crusts, arbuckle mountains, Oklahoma. J. Sediment. Pet. 58 (3), 441–445.

Luque, J.A., Julia, R., 2007. U/Th dating of Quaternary travertines at the middle River Llobregat (NE Iberian peninsula, northwestern Mediterranean). Correlation with sea-level changes. Geol. Acta 5 (1), 109–117.

Maddy, D., Bridgland, D., Westaway, R., 2001. Uplift-driven valley incision and climate-controlled river terrace development in the Thames Valley, UK. Quat. Int. 79, 23–36.

Mahan, S.A., Miller, D.M., Menges, C.M., Yount, J.C., 2007. Late Quaternary stratigraphy and luminescence geochronology of the northeastern Mojave Desert. Quat. Int. 166, 61–78.

Malatesta, L.C., Prancevic, J.P., Avouac, J.-P., 2016. Autogenic entrenchment patterns and terraces due to coupling with lateral erosion in incising alluvial channels. J. Geophys. Res. 121 http://dx.doi.org/10.1002/2015JF003797.

Mallick, R., Frank, N., 2002. A new technique for precise uranium-series dating of travertine micro-samples. Geochim. Cosmochim. Acta 66 (24), 4261–4272.

McCaffrey, R., Nabelek, J., 1998. Role of oblique convergence in the active deformation of the Himalayas and southern Tibet plateau. Geology 26 (8), 691–694.

Meng, X.G., Zhu, D.G., Shao, Z.G., Yang, C.B., Han, J.N., Yu, J., Meng, Q.W., Lu, R.P., 2008. Late Cenozoic stratigraphy and paleomagnetic chronology of the Zanda basin, Tibet, and records of the uplift of the Qinghai-Tibet Plateau. Acta Geol. Sin. 82, 63–72. English edition.

Meyer, M.C., Aldenderfer, M.S., Wang, Z., Hoffmann, D.L., Dahl, J.A., Degering, D., Haas, W.R., Schlütz, F., 2017. Permanent human occupation of the central Tibetan Plateau in the early Holocene. Science 355, 64–67.

Munack, H., Blöthe, J.H., Fülöp, R.H., Codilean, A.T., Fink, D., Korup, O., 2016. Recycling of Pleistocene valley fills dominates 135 ka of sediment flux, upper Indus River. Quat. Sci. Rev. 149, 122–134.

Murari, M.K., Owen, L.A., Dortch, J.M., Caffee, M.W., Dietsch, C., Fuchs, M., Haneberg, W.C., Sharma, M.C., Townsend-Small, A., 2014. Timing and climatic drivers for glaciation across monsoon-influenced regions of the Himalayan–Tibetan orogen. Quat. Sci. Rev. 88, 159–182.

Murphy, M.A., Yin, A., Kapp, P., Harrison, T.M., Lin, D., Guo, J.H., 2000. Southward propagation of the Karakoram fault system, southwest Tibet: timing and magnitude of slip. Geology 28 (5), 451–454.

Murphy, M.A., Yin, A., 2003. Structural evolution and sequence of thrusting in the Tethyan fold-thrust belt and Indus-Yalu suture zone, southwest Tibet. Geol. Soc. Am. Bull. 115 (1), 21–34.

Murray, A.S., Wintle, A.G., 2000. Luminescence dating of quartz using an improved single- aliquot regenerative-dose protocol. Radiat. Meas. 32, 57–73.

Murray, A.S., Wintle, A.G., 2003. The single aliquot regenerative dose protocol : potential for improvements in reliability. Radiat. Meas. 37, 377–381.

Özkul, M., Gokgoz, A., Kele, S., Baykara, M.O., Shen, C.C., Chang, Y.W., Kaya, A., Hancer, M., Aratman, C., Akin, T., Ouml;rus, Z., 2014. Sedimentological and geochemical characteristics of a fluvial travertine: a case from the eastern Mediterranean region. Sedimentology 61 (1), 291–318.

Pan, B.T., Su, H., Hu, Z.B., Hu, X.F., Gao, H.S., Li, J.J., Kirby, E., 2009. Evaluating the role of climate and tectonics during non-steady incision of the Yellow River: evidence from a 1.24 Ma terrace record near Lanzhou, China. Quat. Sci. Rev. 28 (27–28), 3281–3290.

Pedley, H.M., 1990. Classification and environmental models of cool freshwater tufas. Sediment. Geol. 68 (1–2), 143–154.

Pentecost, A., 2005. Travertine. Springer (Berlin).

Perrineau, A., Woerd, J.V.D., Gaudemer, Y., Liu-Zeng, J., Pik, R., Tapponnier, P., Thuizat, R., Rongzhang, Z., 2011. Special Publications. Incision Rate of the Yellow River in Northeastern Tibet Constrained by 10Be and 26Al Cosmogenic Isotope Dating of Fluvial Terraces: Implications for Catchment Evolution and Plateau Building, vol. 353. Geological Society, London, pp. 189–219 (1).

Pratt-Sitaula, B., Burbank, D.W., Heimsath, A., Ojha, T., 2004. Landscape disequilibrium on 1000–10,000 year scales marsyandi river, Nepal, central Himalaya. Geomorphology 58 (1–4), 223–241.

Pratt, B., Burbank, D.W., Heimsath, A., Ojha, T., 2002. Impulsive alluviation during early Holocene strengthened monsoons, central Nepal Himalaya. Geology 30 (10), 911–914.

Prescott, J.R., Hutton, J.T., 1994. Cosmic ray contributions to dose rates for luminescence and ESR dating: large depths and long-term time variations. Radiat. Meas. 23 (1), 497–500.

Rainey, D.K., Jones, B., 2009. Abiotic versus biotic controls on the development of

the fairmont hot springs carbonate deposit, british columbia, Canada. Sedimentology 56 (6), 1832–1857.

Ratschbacher, L., Krumrei, I., Blumenwitz, M., Staiger, M., Gloaguen, R., Miller, B.V., Samson, S.D., Edwards, M.A., Appel, E., 2011. Special Publications. Rifting and Strike-slip Shear in Central Tibet and the Geometry, Age and Kinematics of Upper Crustal Extension in Tibet, vol. 353. Geological Society, London, pp. 127–163 (1).

Rhodes, E.J., 2011. Optically stimulated luminescence dating of sediments over the past 200,000 years. Annu. Rev. Earth. Planet. Sci. 39, 461–488.

Rich, J., Stokes, S., Wood, W., Bailey, R., 2003. Optical dating of tufa via in situ aeolian sand grains: a case example from the Southern High Plains, USA. Quat. Sci. Rev. 22 (10–13), 1145–1152.

Riding, R., 2000. Microbial carbonates: the geological record of calcified bacterial-algal mats and biofilms. Sedimentology 47, 179–214.

Roberts, R.G., Galbraith, R.F., Olley, J.M., Yoshida, H., Laslett, G.M., 1999. Optical dating of single and multiple grains of quartz from Jinmium rock shelter, northern Australia: part II, results and implications. Archaeometry 41 (2), 365–395.

Rumelhart, P.E., Yin, A., Cowgill, E., Butler, R., Qing, Z., Xiao-Feng, W., 1999. Cenozoic vertical-axis rotation of the Altyn Tagh fault system. Geology 27 (9), 819–822.

Ruszkiczay-Rudiger, Z., Fodor, L., Bada, G., Leel-Ossy, S., Horvath, E., Dunai, T.J., 2005. Quantification of Quaternary vertical movements in the central Pannonian Basin: a review of chronologic data along the Danube River, Hungary. Tectonophysics 410 (1–4), 157–172.

Sant'Anna, L.G., Riccomini, C., Rodrigues-Francisco, B.H., Sial, A.N., Carvalho, M.D., Moura, C.A.V., 2004. The Paleocene travertine system of the Itaboraí basin, Southeastern Brazil. J. S. Am. Earth Sci. 18 (1), 11–25.

Saylor, J., DeCelles, P., Gehrels, G., Murphy, M., Zhang, R., Kapp, P., 2010a. Basin formation in the High Himalaya by arc-parallel extension and tectonic damming: Zhada basin, southwestern Tibet. Tectonics 29.

Saylor, J., DeCelles, P., Quade, J., 2010b. Climate-driven environmental change in the Zhada basin, southwestern Tibetan Plateau. Geosphere 6 (2), 74–92.

Saylor, J.E., Quade, J., Dellman, D.L., DeCelles, P.G., Kapp, P.A., Ding, L., 2009. The late Miocene through present paleoelevation history of southwestern Tibet. Am. J. Sci. 309 (1), 1–42.

Schaller, M., Ehlers, T.A., Stor, T., Torrent, J., Lobato, L., Christl, M., Vockenhuber, C., 2016. Timing of European fluvial terrace formation and incision rates constrained by cosmogenic nuclide dating. Earth. Planet. Sci. Lett. 451, 221–231.

Schildgen, T.F., Robinson, R.A.J., Savi, S., Phillips, W.M., Spencer, J.Q.G., Bookhagen, B., Scherler, D., Tofelde, S., Alonso, R.N., Kubik, P.W., Binnie, S.A., Strecker, M.R., 2016. Landscape response to late Pleistocene climate change in NW Argentina: sediment flux modulated by basin geometry and connectivity. J. Geophys. Res. 121 (2), 392–414.

Schulte, L., Julia, R., Burjachs, F., Hilgers, A., 2008. Middle Pleistocene to Holocene geochronology of the river aguas terrace sequence (iberian peninsula): fluvial response to mediterranean environmental change. Geomorphology 98 (1–2), 13–33.

Searle, M., Corfield, R.I., Stephenson, B., McCarron, J., 1997. Structure of the North Indian continental margin in the Ladakh-Zanskar Himalayas: implications for the timing of obduction of the Spontang ophiolite. India-Asia Collis. Deform. Events Himalaya. Geol. Mag 134 (3), 297–316.

Searle, M.P., Pickering, K.T., Cooper, D.J.W., 1990. Restoration and evolution of the intermontane Indus molasse basin, Ladakh Himalaya, India. Tectonophysics 174 (3–4), 301–314.

Sierralta, M., Sandor, K., Melcher, F., Hambach, U., Reinders, J., van Geldern, R., Frechen, M., 2010. Uranium-series dating of travertine from Sutto: implications for reconstruction of environmental change in Hungary. Quat. Int. 222 (1–2), 178–193.

Singh, D., Jain, S.K., Gupta, R.D., 2015. Statistical downscaling and projection of future temperature and precipitation change in middle catchment of Sutlej River Basin, India. J. Earth Syst. Sci. 124 (4), 843–860.

Sinha, A., Cannariato, K.G., Stott, L.D., Li, H.C., You, C.F., Cheng, H., Edwards, R.L., Singh, I.B., 2005. Variability of southwest Indian summer monsoon precipitation during the Boiling-Allerod. Geology 33 (10), 813–816.

Srivastava, P., Rajak, M.K., Singh, L.P., 2009. Late Quaternary alluvial fans and paleosols of the Kangra basin, NW Himalaya: tectonic and paleoclimatic implications. Catena 76 (2), 135–154.

Srivastava, P., Tripathi, J.K., Islam, R., Jaiswal, M.K., 2008. Fashion and phases of late Pleistocene aggradation and incision in the alaknanda river valley, western Himalaya, India. Quat. Res. 70 (1), 68–80.

Starkel, L., 2003. Climatically controlled terraces in uplifting mountains areas. Quat. Sci. Rev. 22 (20), 2189–2198.

Strecker, M.R., Hilley, G.E., Arrowsmith, J.R., Coutand, I., 2003. Differential structural and geomorphic mountain-front evolution in an active continental collision zone: the northwest Pamir, southern Kyrgyzstan. Geol. Soc. Am. Bull. 115 (2), 166–181.

Tadono, T., Ishida, H., Oda, F., Naito, S., Minakawa, K., Iwamoto, H., 2014. Precise global DEM generation by ALOS PRISM. ISPRS annals of the photogrammetry. Remote Sens. Spat. Inf. Sci. 2 (4), 71.

Tan, H.B., Zhang, Y.F., Zhang, W.J., Kong, N., Zhang, Q., Huang, J.Z., 2014. Understanding the circulation of geothermal waters in the Tibetan Plateau using oxygen and hydrogen stable isotopes. Appl. Geochem 51, 23–32.

Taylor, M., Yin, A., Ryerson, F.J., Kapp, P., Ding, L., 2003. Conjugate strike-slip faulting along the Bangong-Nujiang suture zone accommodates coeval east-west extension and north-south shortening in the interior of the Tibetan Plateau.

Tectonics 22 (5), 1044.

Thakur, V.C., Joshi, M., Sahoo, D., Suresh, N., Jayangondapermal, R., Singh, A., 2014. Partitioning of convergence in Northwest Sub-Himalaya: estimation of late Qua-ternary uplift and convergence rates across the Kangra reentrant, North India. Int. J. Earth Sci. 103, 1037—1056.

Tong, W., Liao, Z., Liu, S., Zhang, Z., You, M., Zhang, M., 2000. Thermal springs in Tibet. Science Press, Beijing (in Chinese).

Van Campo, E., Gasse, F., 1993. Pollen- and diatom-inferred climatic and hydro-logical changes in Sumxi Co basin (western Tibet) since 13,000 yr B.P. Quat. Res. 39 (3), 300—313.

Vance, D., Bickle, M., Ivy-Ochs, S., Kubik, P.W., 2003. Erosion and exhumation in the Himalaya from cosmogenic isotope inventories of river sediments. Earth Planet. Sci. Lett. 206 (3—4), 273—288.

Vandenberghe, J., 2002. The relation between climate and river processes, land-forms and deposits during the Quaternary. Quat. Int. 91, 17—23.

Wang, A., Smith, J.A., Wang, G.C., Zhang, K.X., Xiang, S.Y., Liu, D.M., 2009. Late Quaternary river terrace sequences in the eastern Kunlun Range, northern Tibet: a combined record of climatic change and surface uplift. J. Asian Earth Sci. 34 (4), 532—543.

Wang, S.F., Blisniuk, P., Kempf, O., Fang, X.M., Chun, F., Wang, E., 2008a. The basin-range system along the south segment of the Karakorum fault zone, Tibet. Int. Geol. Rev. 50 (2), 121—134.

Wang, S.F., Zhang, W.L., Fang, X.M., Dai, S., Kempf, O., 2008b. Magnetostratigraphy of the Zanda basin in southwest Tibet Plateau and its tectonic implications. Chin. Sci. Bull. 53 (9), 1393—1400.

Wang, X., Vandenberghe, J., Yi, S., Van Balen, R., Lu, H., 2015. Climate-dependent fluvial architecture and processes on a suborbital timescale in areas of rapid tectonic uplift: an example from the NE Tibetan Plateau. Glob. Planet. Change 133, 318—329.

Wang, Z., Meyer, M.C., Hoffmann, D.L., 2016. Sedimentology, petrography and early diagenesis of a travertine—colluvium succession from Chusang (southern Tibet). Sediment. Geol. 342, 218—236.

Wedepohl, K.H., 1995. The composition of the continental-crust. Geochim. Cos-mochim. Acta 59 (7), 1217—1232.

Wegmann, K.W., Pazzaglia, F.J., 2002. Holocene strath terraces, climate change, and active tectonics: the Clearwater River basin, Olympic Peninsula. Wash. State. Geol. Soc. Am. Bull. 114 (6), 731—744.

Wegmann, K.W., Pazzaglia, F.J., 2009. Late Quaternary fluvial terraces of the Romagna and Marche Apennines, Italy: climatic, lithologic, and tectonic con-trols on terrace genesis in an active orogen. Quat. Sci. Rev. 28 (1—2), 137—165.

Wintle, A.G., 1997. Luminescence dating: laboratory procedures and protocols. Radiat. Meas. 27 (5), 760—817.

Wünnemann, B., Yan, D., Ci, R., 2015. Morphodynamics and lake level variations at Paiku Co, southern Tibetan Plateau, China. Geomorphology 246, 489—501.

Yao, T.D., Masson-Delmotte, V., Gao, J., Yu, W.S., Yang, X.X., Risi, C., Sturm, C., Werner, M., Zhao, H.B., He, Y., Ren, W., Tian, L.D., Shi, C.M., Hou, S.G., 2013. A review of climatic controls on δ18O in precipitation over the Tibetan Plateau: observations and simulations. Rev. Geophys 51 (4).

Yin, A., 2000. Mode of Cenozoic east-west extension in Tibet suggesting a common origin of rifts in Asia during the Indo-Asian collision. J. Geophys. Res. 105 (B9), 21745—21759.

Yin, A., Harrison, T.M., 2000. Geologic evolution of the Himalayan-Tibetan orogen. Annu. Rev. Earth Planet. Sci. 28, 211—280.

Yin, A., Harrison, T.M., Murphy, M.A., Grove, M., Nie, S., Ryerson, F.J., Feng, W.X., Le, C.Z., 1999. Tertiary deformation history of southeastern and southwestern Tibet during the Indo-Asian collision. Geol. Soc. Am. Bull. 111 (11), 1644—1664.

Zentmyer, R., Myrow, P.M., Newell, D.L., 2008. Travertine deposits from along the south tibetan fault system near Nyalam. Tibet. Geol. Mag. 145 (6), 753—765.

Zhang, K.X., Wang, G.C., Ji, J.L., Luo, M.S., Kou, X.H., Wang, Y.M., Xu, Y.D., Chen, F.N., Chen, R.M., Song, B.W., Zhang, J.Y., Liang, Y.P., 2010. Paleogene-Neogene strati-graphic realm and sedimentary sequence of the Qinghai-Tibet Plateau and their response to uplift of the plateau. Sci. China Earth Sci. 53 (9), 1271—1294.

Zhu, L.P., Lu, X.M., Wang, J.B., Peng, P., Kasper, T., Daut, G., Haberzettl, T., Frenzel, P., Li, Q., Yang, R.M., Schwalb, A., Mausbacher, R., 2015. Climate change on the Tibetan Plateau in response to shifting atmospheric circulation since the LGM. Sci. Rep. 5, 13318,. http://dx.doi.org/10.1038/srep13318.

Zhu, S., Wu, Z.H., Zhao, X.T., Li, J.P., Xiao, K.Y., 2014. Ages and genesis of terrace flights in the middle reaches of the Yarlung Zangbo river, tibetan plateau, China. Boreas 43 (2), 485—504.